Composites Part B 266 (2023) 111036

Contents lists available at ScienceDirect

Composites Part B

journal homepage: www.elsevier.com/locate/compositesb

Experimental and numerical investigation of the intra-ply shear behaviour of unidirectional prepreg forming through picture-frame test

Hao Yuan, Muhammad Khan *, Connie Qian, Neil Reynolds, Kenneth Kendall

Automotive Composites Research Centre, Warwick Manufacturing Group, University of Warwick, Coventry, CV4 7AL, United Kingdom

ARTICLE INFO

Handling Editor: Prof. Ole Thomsen

Keywords:
Prepreg processing
Intra-ply shear
Picture-frame test
Digital image correlation
Hypoelastic model

ABSTRACT

Intra-ply shear behaviour of uncured composite plies strongly influences component quality in advanced manufacturing processes such as prepreg compression moulding (PCM) and double diaphragm forming (DDF). This study investigates a straightforward method to characterise the intra-ply shear behaviour of a carbon fibre/epoxy UD prepreg using a specially designed picture-frame rig, by which specimens can be tested without involving inter-ply shear as would normally be observed in cross-plied UD prepreg stacks. Applying the proposed method, it is seen that specimens tend to suffer transverse buckling/wrinkling and local fibre-splitting at large shear strains. 3D digital image correlation (DIC) and a non-contacting video extensometer were utilised to determine the shear strain distribution throughout the test and particularly to determine the onset of out-of-plane deformations such that the trellis shear deformation portion of the test can be identified. The obtained shear stress-strain results show a temperature- and rate-dependent viscoelastic response, with the greatest influence from the temperature. The obtained in-plane shear properties were applied in the numerical simulation of the picture frame test based on a hypoelastic law. Although the predicted reaction forces are greater than experimental results at high strains due several factors including local fibre-splitting, a good agreement overall between physical test data and simulation results is seen for all test conditions. Finally, it is demonstrated that major advantages of the proposed test with respect to the conventional picture-frame test are that only load-extension data are required from the trellis shear experiment to calculate accurately the intra-ply shear stress-strain relationship and that the deformation rate can be easily controlled.

1. Introduction

The demand for lightweight structures has increased significantly in recent years with development of electric vehicles and sustainable transportation. High performance composite materials are promising candidates for lightweight structures due to their superior mass-normalised mechanical properties. Recent advances in fast cure thermosetting resin technology make high volume manufacturing of structural composites possible through processes such as prepreg compression moulding (PCM) and double-diaphragm die-match forming (3DF) [1,2]. Such processes involve a preforming stage where uncured stacked flat prepreg plies are warm-formed into desired three-dimensional shapes under pressure. Different types of defects can occur during this step with wrinkling being the most severe, and these cause significant reduction in the mechanical performance of final parts [3]. In the automotive sector, components are often complex in geometry, making it challenging to predict accurately the deformation of materials using forming simulation. Therefore, the development and application of appropriate characterisation methods to understand and characterise underlying fundamental deformation mechanisms of such materials during forming is crucial in creating robust process modelling tools to deliver optimised and repeatable high-volume processes.

For high-volume processes such as PCM and 3DF, major deformation mechanisms are intra-ply/in-plane shear, inter-ply shear/friction and out-of-plane bending. Intra-ply shear is a predominant deformation mode when forming complex structures with double-curvature geometries [4]. This deformation mode for woven prepregs has been studied extensively both experimentally [5–9] and via simulations [10–14]. The shear rate of the material can reach above 0.16/s at small area (4% of the area in a double-dome forming) whereas the majority of the areas experience a shear strain rate less than 0.02/s [2]. The non-linear shear stress-strain relationship is usually measured in these studies and the shear locking angle is usually identified as the formability limit for the woven prepreg where fibre tows themselves start to get compacted as

* Corresponding author.
E-mail address: m.a.khan@warwick.ac.uk (M. Khan).

https://doi.org/10.1016/j.compositesb.2023.111036
Received 22 June 2023; Received in revised form 11 September 2023; Accepted 5 October 2023
Available online 5 October 2023

gaps between them are already fully closed. However, this shear locking angle does not exist for unidirectional (UD) prepreg, a material form that can offer better quality and mechanical properties for the composite parts due to zero crimp. The intra-ply shear occurs in form of the relative slippage between individual fibres and tows along the axial fibre direction in UD prepregs during forming [15]. Nevertheless, UD prepregs are far more compliant than woven prepregs in the direction transverse to fibres. This poses some difficulties when considering suitable methods for characterising intra-ply shear behaviour where trellis shear deformation and material integrity must be guaranteed. Further, the presence of uncured resin in UD prepregs plays a key role in affecting the adhesion between fibres at different testing conditions. Therefore, the candidate testing procedure must also allow for the characterisation to be performed conveniently across an industrially relevant range of deformation rates and temperatures.

Much effort has already been expended by different research groups towards tackling the challenges involved in the intra-ply shear characterisation for UD prepregs. In an early attempt, Groves developed a testing method in which UD prepregs are placed between two parallel platens on a rheometer and the shear is induced by the rotation of one of the platens in oscillation or steady motion [16]. Both intra-ply and inter-ply shear were characterised together as an isotropic response for cross-plied laminate specimens in this test. A redesigned off-centre UD specimen was adopted in a later study [17] to test two deformation modes separately; however, converting the results for use in modelling remains challenging due to the non-uniform distribution of shear deformation along the radial coordinates. Instead of rotating motion, Scobbo and Nakajima developed the parallel-shear-plate test that induces shear deformation through a translational motion of the testing rig [18]. In this test, two consolidated UD prepreg laminates are placed in the gap of three parallel platens and two outer platens on both sides are fixed while the central platen oscillating translationally [18] or being pulled out at a constant speed for steady shear characterisation [19]. A simplified alternative test was used by Wheeler and Jones to test the stacked UD prepreg specimen between a fixed platen and a moving platen that induces the dynamic translational motion [20–22]. However, the maximum shear rate tested in these methods (up to 100/s) were not relevant to the process investigated in this study and the major challenge of such parallel-shear-plate tests is their susceptibility in developing confounding inter-ply shear/friction forces occurring locally at resin rich regions in ply-ply interfaces. The same issue of inter-ply shear could also occur in the vee-bending test [23] which is similar to the short beam shear test for cured composites.

The most commonly used methods for in-plane shear characterisation for biaxial fabrics (i.e. picture-frame [24,25] and bias-extension tests [26–28]) have also been adopted for UD prepregs. A wide range of shear strain rates (0.001–3.82/s) relevant to different manufacturing processes were achieved through these two approaches by simply adjusting the crosshead speed of the testing machine. However, to the best of the authors' knowledge, only cross-plied UD laminates were used in all existing studies based on these two methods to accommodate the unidirectionality of the material. Consequently, the issue of ambiguity regarding a combined response resulting from both from intra-ply shear and inter-ply friction arises again at the cross-over region of two plies for these tests. More recently, Haanappel and Akkerman designed a torsion bar test that involves twisting a prismatic specimen made from 80 plies of UD prepregs through the standard torsion fixture on a rheometer [29]. The kinematics of the test was derived analytically to separate axial and shear contributions to the measured force. However, representative large strains and high strain rates cannot be achieved at the same time due to the limitation of the rheometer. Potter made an initial attempt to address the in-plane deformation of UD prepregs via the off-axis tensile test and laminated prepreg specimens with different fibre angles between 15° and 90° [30]. The strain was found to dominate in a region at the centre of the specimen and the size of this highly strained region can be tailored by adjusting specimen dimensions and off-axis angles. Recently, this test was complemented by the use of digital image correlation (DIC) for strain measurement of this localised deformation band [15]. The stresses were resolved into shear and transverse extension components for the test with a 10° off-axis angle and the shear stress-strain relationship were derived for the use in simulation [31]. However, shear strain measurement relies on the use of DIC which can be time-consuming for a large test campaign for the new materials.

This study proposes the use of only slightly modified popular picture-frame apparatus for intra-ply shear characterisation of UD prepregs, relying on its simplicity and convenience in terms of both experimental methodology and data analysis where only load-extension data are required. The modified picture-frame test setup allows two separately clamped UD plies to undergo intra-ply shear deformation, without the contribution of confounding inter-ply shear responses observed in the standard picture-frame test with cross-plied specimens. In terms of the scope of this study, the next section presents the details of the test set up, an overview of the test programme and most importantly, the feasibility and applicability of picture-frame test for UD prepreg in-plane shear characterisation. Then results are presented from the exploration of specimen size effects and the shear stress-strain results from three different temperatures (i.e. 21 °C, 50 °C and 80 °C) and two shear rates (i.e. 0.00267/s and 0.0107/s). A finite element (FE) model replicating the picture frame test was set up in ABAQUS/Explicit and the experimentally obtained shear stress-strain data were used as the in-plane shear property in this model. A comparison of the load results was made between the physical test and the simulation to verify the proposed intra-ply shear characterisation method and to validate the implementation of the obtained experimental data in the simulation model that was based on a hypoelastic law.

2. Materials and methods

2.1. Materials

The material used for the intra-ply shear characterisation investigations in this study is PYROFIL™ unidirectional carbon fibre/epoxy thermoset prepreg from Mitsubishi Rayon Co., Ltd (Fig. 1 (a)). The prepreg is made of carbon fibres with a 15k tow size and the epoxy resin content by weight is 30%. This material is specially designed for automated automotive processes and has a 5-min curing cycle at 140 °C and 8 MPa pressure in the compression moulding process. The log-linear graph in Fig. 1 (b) shows the viscosity of epoxy resin in the prepreg as a function of temperature. The recommended temperature for preforming the material is 80 °C, at which there is no significant change of the degree-of-cure of the resin.

2.2. Test setup and test conditions

As discussed, previous intra-ply shear characterisation studies via picture-frame testing have typically used cross-plied UD prepreg specimens, and these introduce possible inter-ply shear/friction between ply boundaries stacked orthogonally. This study adopts a purpose designed testing rig (Fig. 2) that ensures a gap between individual ply level specimens that are clamped perpendicularly, therefore eliminating inter-ply shear deformation response. The length of the frame rig is 150 mm and the width of four grips is 20 mm. All specimens tested in the study were fixed by grips through two bolts and the third bolt hole in the middle of the grip was not used. A specially made steel angle was used to prevent misalignment when mounting the specimen. The rig is installed on an INSTRON 5985 universal testing machine and a load cell of 1 kN capacity was used.

To determine the effect of the process temperature and forming rate on the viscous epoxy resin, the test was performed at three different temperatures (room temperature (~21 °C), 50 °C and 80 °C) and two constant crosshead speeds (*low*, 0.25 mm/s and *high*, 1 mm/s) using an INSTRON environmental chamber. These candidate test conditions were

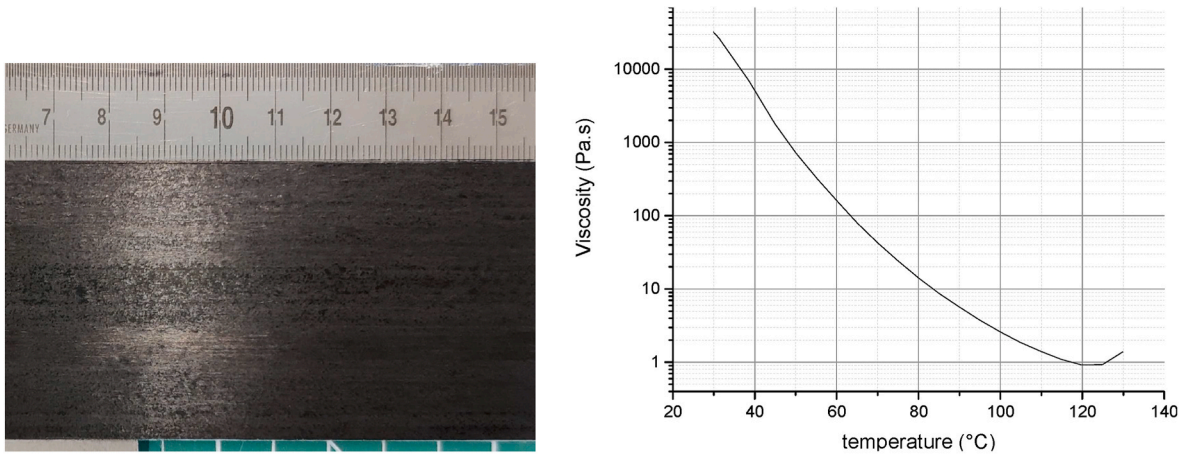

Fig. 1. (a) Images of uncured PYROFIL™ UD prepreg and (b) viscosity of the epoxy in PYROFIL™ prepreg as a function of temperature from material supplier's data.

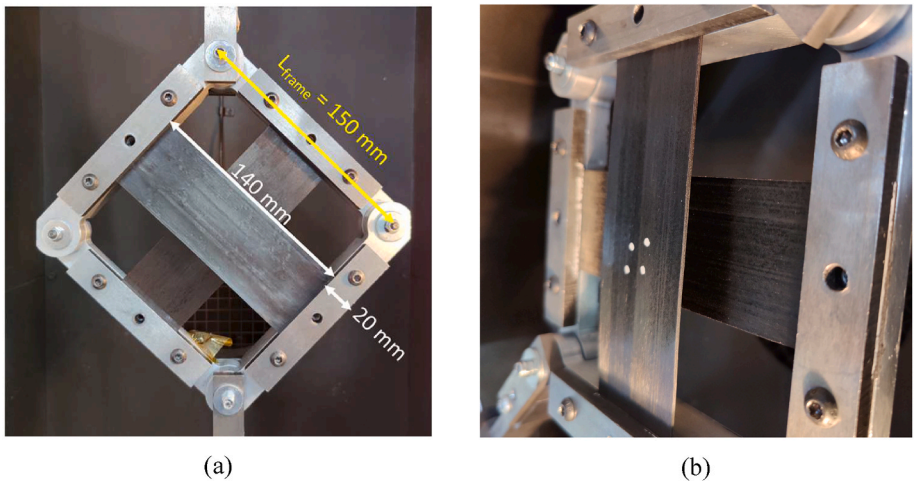

Fig. 2. (a) picture-frame testing rig designed for UD prepreg and (b) a gap between specimens in two orientations.

derived from commonly adopted industrial processing conditions for thermoset prepreg, thus allowing the effects of relevant process parameters on material intra-ply shear behaviour to be investigated [32]. Meanwhile, to differentiate between apparent (system-induced) responses and fundamental material behaviour, specimens with different thicknesses and widths were tested across a range of the above testing conditions. As the force at higher temperature is significantly lower, only the room temperature condition was selected for the tests of the variation of specimen width to highlight any differences in the results more easily, especially for specimens with smaller width, hence an appropriate specimen width can be selected for completing the full test matrix. The complete set of unique test conditions used in this study are summarised in Table 1. Five repeats were done at each unique test condition and at least three sets of consistent data were selected from each condition for analysis. It is worth noting that the dry run (pulling the picture-frame rig without specimens) was performed at each test condition to determine the force required to deform the empty rig, hence the influence of this force can be subtracted when processing the data.

The rectangular shaped specimens with a length of 180 mm and different widths were cut from the roll using a ZUND S3 CNC cutter to minimise the fibre misalignment errors during the preparation. UD specimens with 3 plies and 5 plies were produced by laying up cut plies at the same orientation and debulking them under the vacuum (~1 bar) for 90 min to minimise the influence of resin rich regions at the ply-ply

Table 1
Test matrix for the investigation on size effects, temperature and deformation rate.

		Temperature		
		21 °C	50 °C	80 °C
Crosshead speed	Low 0.25 mm/s	Dry run 1 ply – 50 mm 1 ply – 25 mm 1 ply – 15 mm 3 plies – 50 mm 5 plies – 50 mm	Dry run 1 ply – 50 mm 3 plies – 50 mm 5 plies – 50 mm	Dry run 1 ply – 50 mm 3 plies – 50 mm 5 plies – 50 mm
	High 1 mm/s	Dry run 1 ply – 50 mm 3 plies – 50 mm 5 plies – 50 mm	Dry run 1 ply – 50 mm 3 plies – 50 mm 5 plies – 50 mm	Dry run 1 ply – 50 mm 3 plies – 50 mm 5 plies – 50 mm

Note: Each entry denotes the specimen configuration tested (i.e. number of plies – specimen width).

interface. Thickness measurements for untested specimens were taken at five different locations using a digital calliper for each thickness after cured in the oven using supplier recommended conditions. The nominal thicknesses were found to be 0.27 mm, 0.78 mm and 1.22 mm for specimens with 1 ply, 3 plies and 5 plies, respectively.

2.3. Overview of the picture frame test

In a series of initial trial tests, the deformed specimen showed wrinkling/buckling transverse to the fibre direction at an increased shear angle (Fig. 3 (a)). As illustrated in Fig. 3 (b), this is attributed to the small gradual reduction in specimen width during the test causing some levels of compaction in the transverse direction. The specimen width, w, during the test follows:

$$w = w_0 \sin 2\theta = w_0 \bullet \sin\left(\frac{\pi}{2} - \gamma\right) \tag{1}$$

where w_0 is the specimen initial width, θ is half of the frame angle and γ is the shear angle as indicated in Fig. 3 (b). As demonstrated in Ref. [33], a uniform shear deformation can be obtained within the specimen in a picture-frame test and the shear angle of specimen can be readily determined as:

$$\gamma = \frac{\pi}{2} - 2 \bullet \cos^{-1}\left(\frac{\sqrt{2}L_{\text{frame}} + d}{2 \bullet L_{\text{frame}}}\right) \tag{2}$$

where L_{frame} is the frame length (150 mm for current test rig) and d is the crosshead displacement of the testing machine. As shown in Fig. 4 (a), the reduction of specimen width resulting from the first 10° of shear deformation is only 4.12%, corresponding to a 16.50 mm crosshead displacement. Therefore, all specimens were only tested up to 20 mm crosshead displacement (12.25° shear angle) to limit the level of transverse compaction.

It was demonstrated in Ref. [5] that the shear rate $\dot{\gamma}$ during the picture-frame test can be expressed as:

$$\dot{\gamma} = \frac{\dot{d}}{L_{\text{frame}} \bullet \sin\theta} = \frac{2\dot{d}}{\left(2{L_{\text{frame}}}^2 - 2\sqrt{2}L_{\text{frame}} \bullet d - d^2\right)^{\frac{1}{2}}} \tag{3}$$

where $\dot{d}$ denotes the crosshead speed of the testing machine. The resultant shear rate versus crosshead displacement corresponding to the two fixed crosshead speeds used in this study are plotted in Fig. 4 (b). The change in shear rate across the 20 mm crosshead displacement range is relatively small, hence the shear rate during the test in this study was considered as constant for the two fixed crosshead speeds. The interceptions of the linearly fitted zero-gradient lines (0.00267 s^{-1} and 0.0107 s^{-1}) are referred as the nominal shear rates for *low* (0.25 mm/s) and *high* (1 mm/s) speed tests respectively.

2.4. Comparison between the proposed test and the standard picture-frame test

As part of the exploration tests, the standard picture-frame test with the cross-plied specimens was performed on the back side of the same test rig where specimens in two orientations are in-contact at the overlapping region (Fig. 5 (a)). One-ply cross-plied specimens tested at 0.25 mm/s crosshead speed and three different temperatures are presented in Fig. 5 (b)–(d), showing no wrinkling in the overlapping region. However, the wrinkling can still be observed in the non-cross-plied regions ("arms"). Further, a comparison of the test-results from the cross-plied and separated UD specimens have been shown in Fig. 6. The recorded load-extension curves for cross-plied specimens show significantly higher forces at large extensions (even with less than 36% of specimen area overlapping), especially for high temperature tests.

The higher force for cross-plied specimens can attributed to the rotational friction on the interface between plies of different orientation, which does not occur in the separated UD specimens. As the tackiness of the resin increases with the temperature, this effect can make a greater contribution to the measured force in the high temperature tests, causing the curves to deviate from the ones for separated specimens at a much earlier stage (Fig. 6 (c) and (d)). Further, higher thickness at the overlapping region and fibres in the second orientation in the cross-plied specimen increase the specimen's resistance to transverse buckling. Nevertheless, additional out-of-deformations or a different mode of buckling can occur in the non-cross-plied arms regions by comparing the specimens in Fig. 5 (b) to Fig. 3 (a), which leads to the higher force observed in cross-plied specimens. This comparison highlights the differences between the proposed test and a standard picture-frame test and emphasises the need for such a method in characterising the intra-ply shear properties for the UD prepreg.

2.5. Overview of the specimen behaviour

The uniform in-plane strain distribution of the specimen for a picture-frame test can be interrupted by the wrinkling, inducing additional deformation modes. Therefore, the onset of wrinkling needs to be determined to ensure the valid data region is selected with minimum effects from arising out-of-plane deformations. A GOM 12 M DIC system was adopted to calculate the deformation and to ensure the validity of the selected datasets from the initial exploratory tests (Fig. 7). A matt-finish white acrylic paint was sprayed directly onto the specimen surface to create a high contrast stochastic speckle pattern for DIC. The

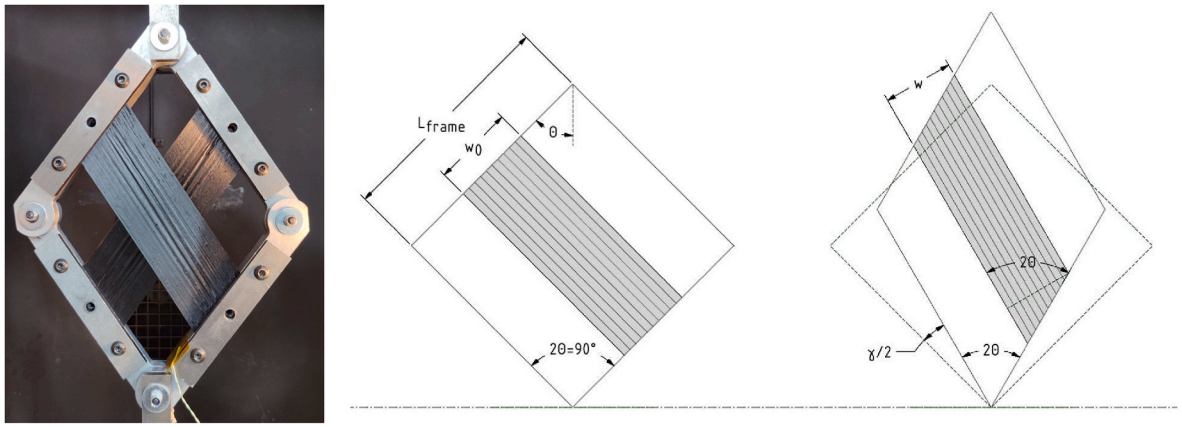

Fig. 3. (a) Wrinkling shown at large shear angle (21 °C, 0.25 mm/s); (b) schematic illustration of specimen width reduction in the test.

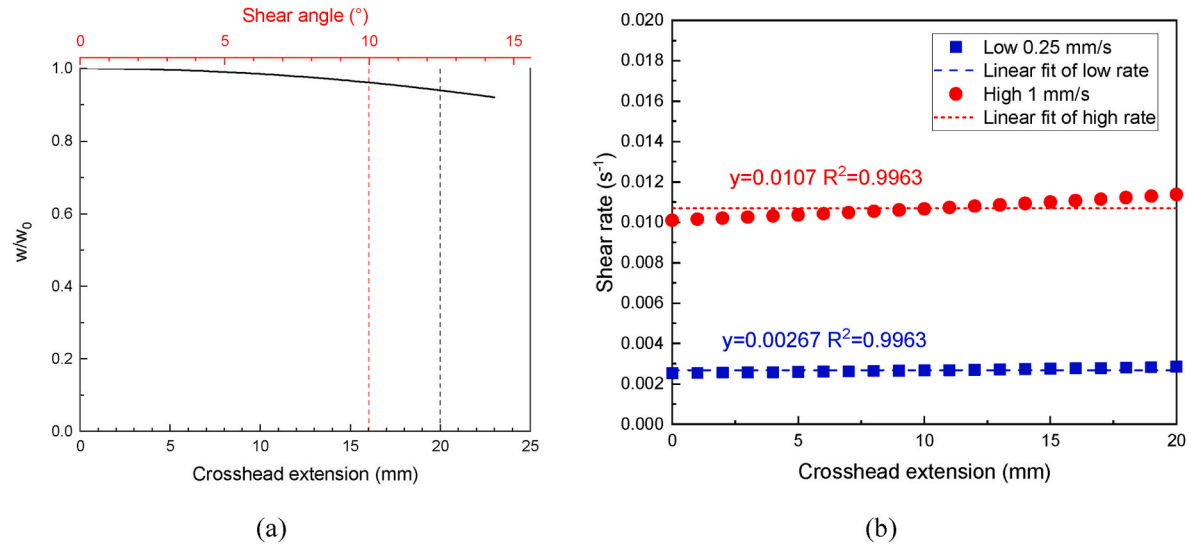

Fig. 4. (a) The ratio of specimen width during the test and initial specimen width vs. crosshead displacement/shear angle, (b) shear rate vs. crosshead displacement for two crosshead speeds used.

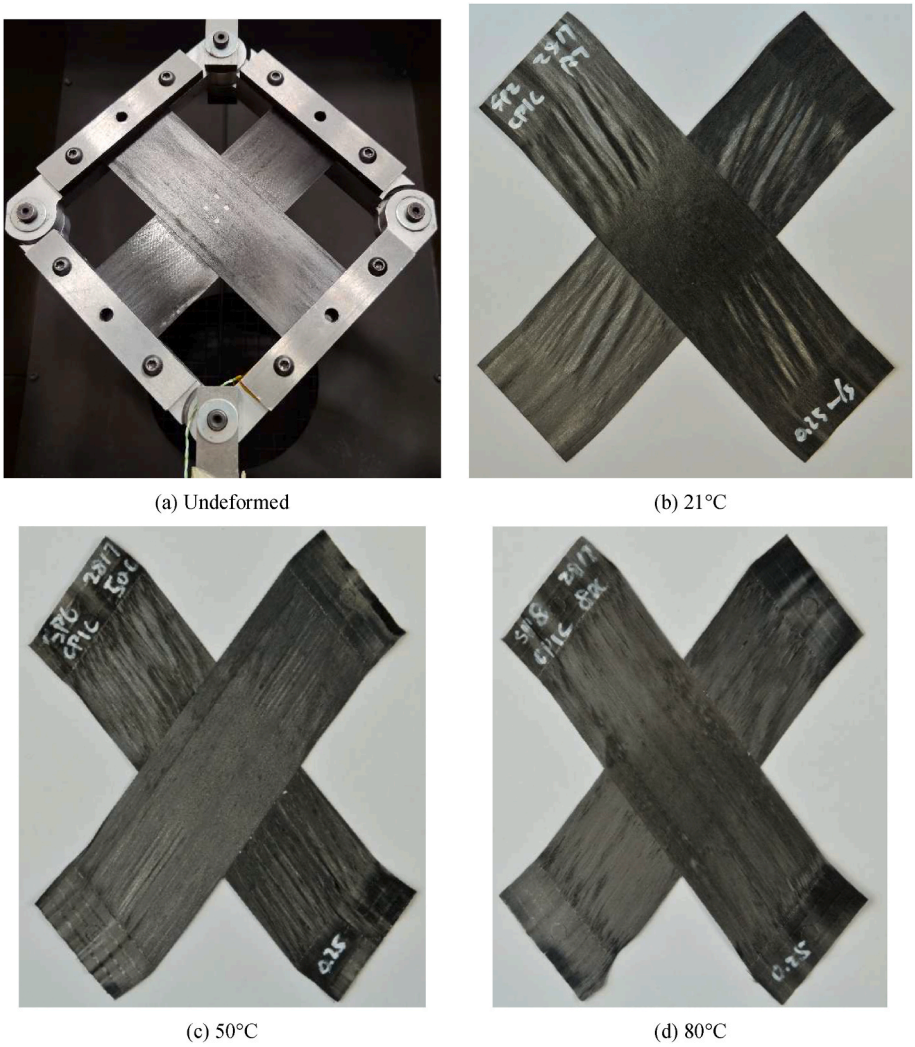

Fig. 5. (a) The standard picture-frame test with cross-plied UD prepreg specimens (1-ply, undeformed) and the specimens after the test at the (b) 21 °C, (c) 50 °C and (d) 80 °C temperature and 0.25 mm/s test speed.

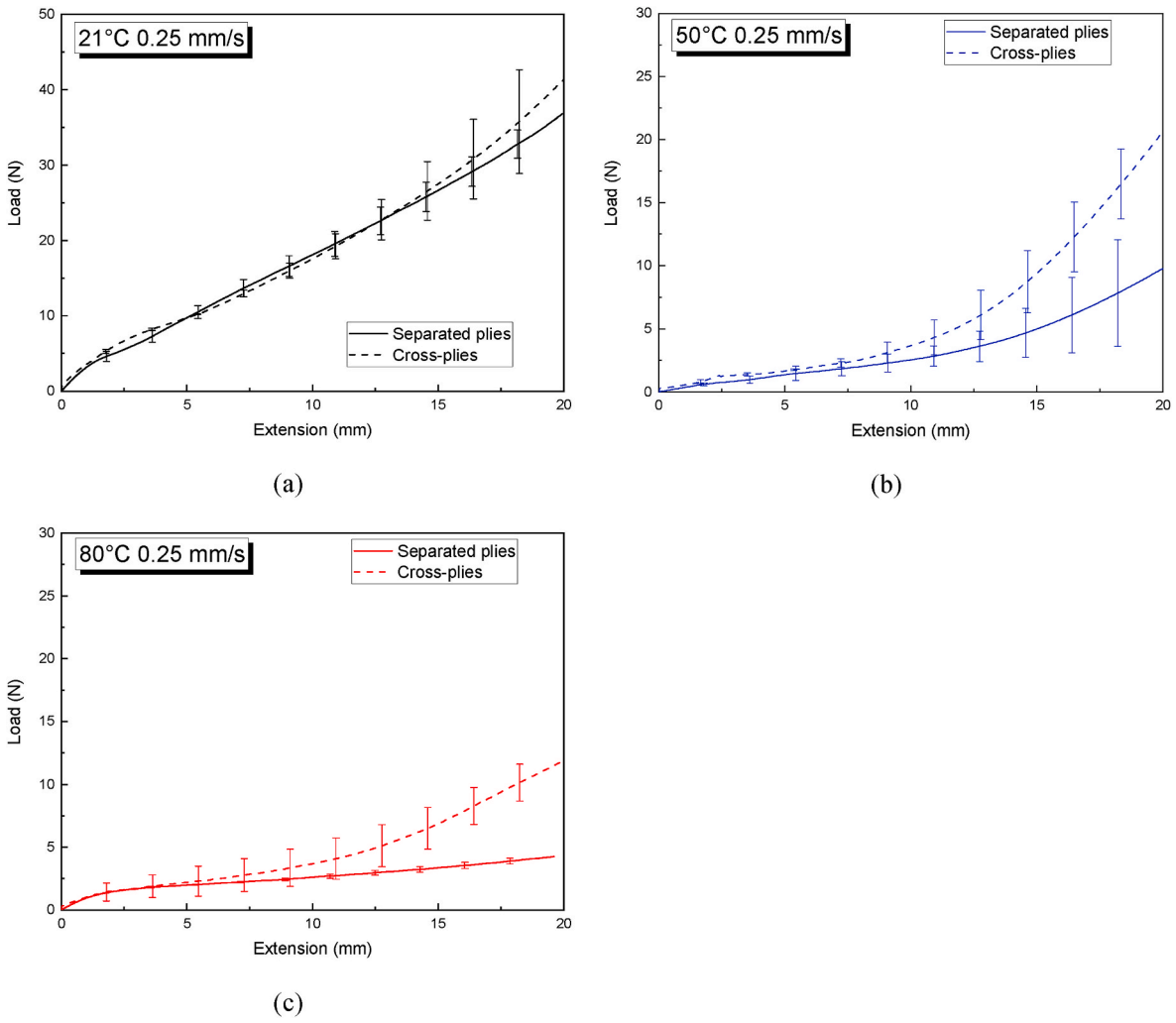

Fig. 6. A comparison of load-extension curves between proposed picture-frame test with separated plies (solid lines) and standard picture-frame test with cross-plied specimens (dashed lines) at 0.25 mm/s test speed and three different temperatures.

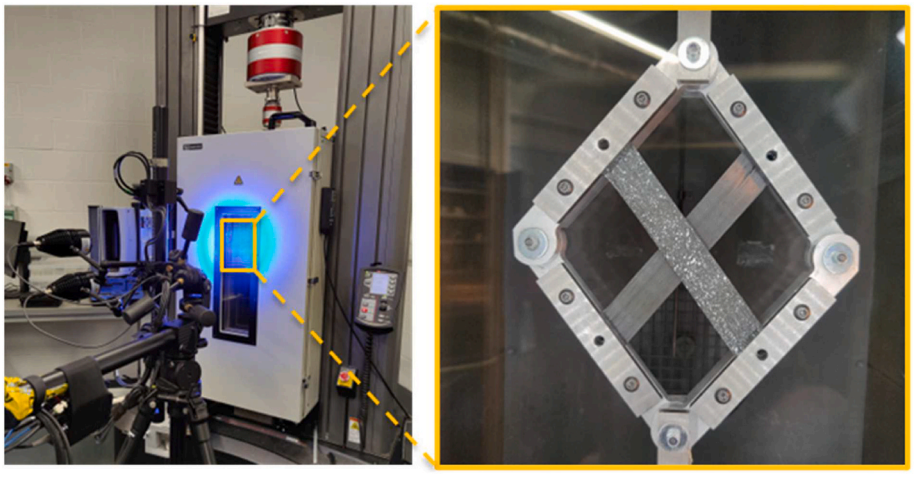

Fig. 7. Test setup with DIC.

recorded DIC full-field deformation data were synchronised with load and extension results from INSTRON testing machine in real-time via an analogue-digital converter. The influence of the acrylic paint on material response was evaluated in trial tests via comparison of load-extension curves of painted and unpainted specimens and results confirmed minimal effects from the paint.

The full-field strain results in post-processing software GOM Aramis v6 are expressed in terms of a global coordinate system which is fixed to

the sensors. Due to the rigid body rotation of fibres occurring throughout the test, the x-axis of the coordinate system should be aligned with the fibre direction to generate correct strain maps. The transformation of the coordinate system was performed directly in GOM Aramis for each frame of DIC results based on the rotation angle of testing rig measured using ImageJ image processing software [34] and the nominal shear angle was derived from this rotation angle using Eq. (2). Fig. 8 shows in-plane shear angle and out-of-plane deformation results from DIC at different stages during the test (the crosshead displacement is indicated for each deformation map). A relatively uniform shear angle distribution can be seen in initial stages of the test as indicated by the shear angle histogram in the legend. The uniformity of shear deformation decreases and the standard deviation (*SD*) of measured shear angle increases as the specimen is further deformed and the out-of-plane deformation becomes obvious.

Fig. 9 (a) shows the history of out-of-plane deformation along the centre line of specimen (section line Section 1 in Fig. 8) extracted from the DIC data at increasing nominal shear angles. It must be noted that as UD prepregs are extremely compliant in the direction transverse to fibres, it is almost impossible to manually mount the specimen onto the rig while keeping it completely flat. The small out-of-plane deformation at the beginning stage (<1° nominal shear angle) is attributed to this compliance. At shear angles between 4° and 5°, a sudden change in the deformed shape and a corresponding decrease in specimen width

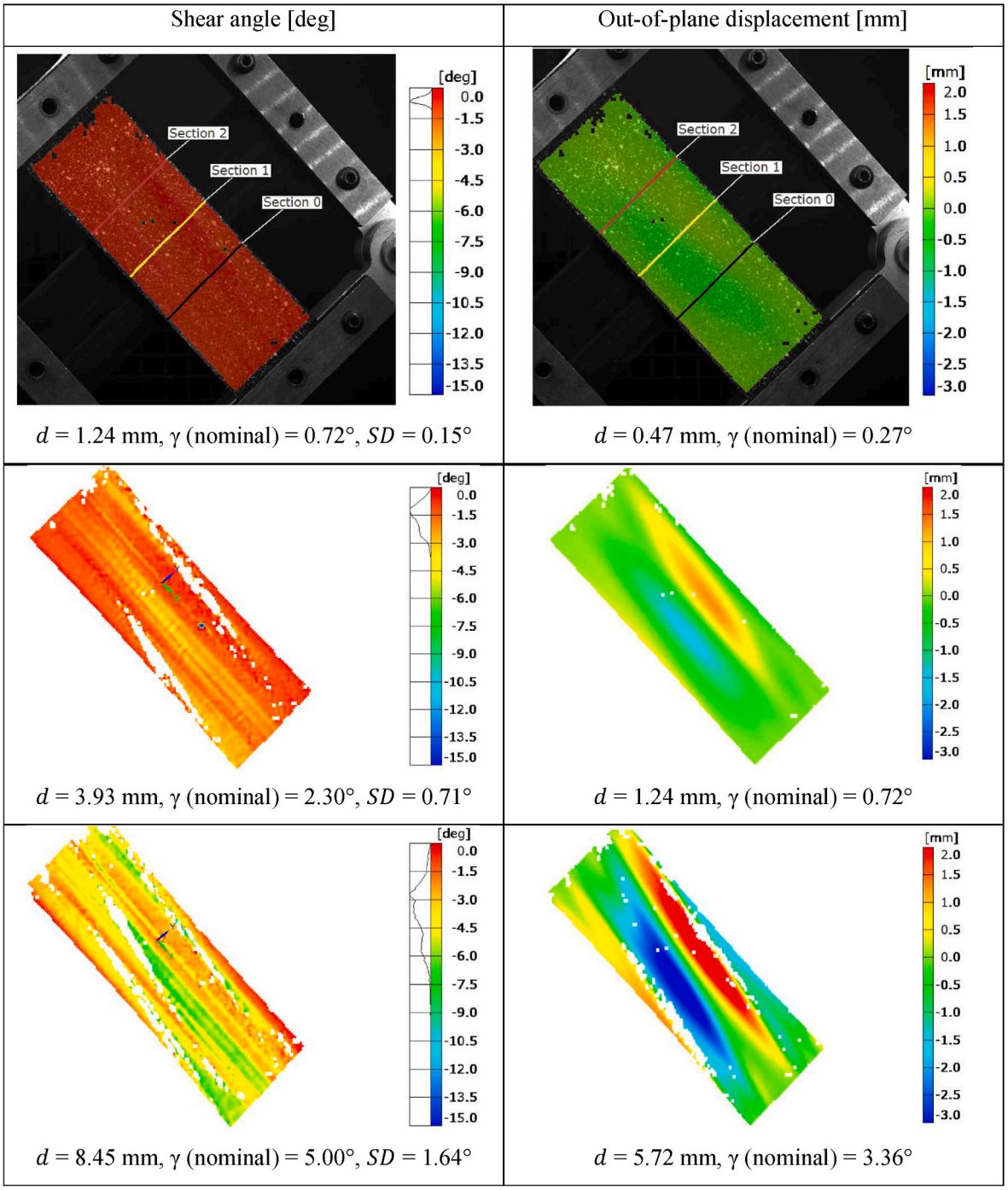

Fig. 8. DIC analysis results: shear angle and out-of-plane deformation for a specimen with 1 ply and 50 mm width tested at 21 °C and low shear rate (0.00267 s^{-1}) (*SD* is the standard deviation of the shear angle results measured by DIC).

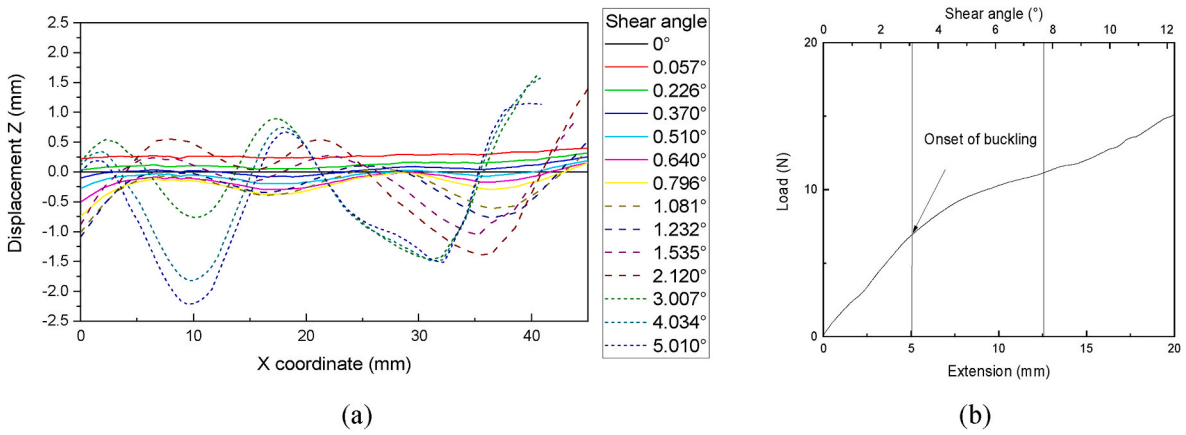

Fig. 9. (a) Out-of-plane deformation history along centre section line obtained from DIC and (b) load-extension curve of a specimen with 1ply and 50 mm width tested at 21 °C and low shear rate (0.00267 s^{-1}).

suggest the onset of transverse buckling. Further evidence of this phenomenon can be found from the representative load-extension curve (Fig. 9 (b)), as the apparent stiffness reduces after the initial linear section. Following this, the representative curve shows a further stiffness increase, possibly caused by the spurious tensile force from fibre misalignment. The onset of transverse buckling is expected to vary between test configurations as the resistance to buckling is dependent on resin viscosity and specimen geometry. In this study the onset of buckling for each test was not determined for every test using DIC as there were difficulties in using the DIC system to obtain reliable photogrammetric measurements through a double-glazed window of the environmental chamber for the tests at elevated temperatures.

2.6. In-situ shear strain measurement

For tests without the aid of DIC, it is important to employ another viable experimental approach that can measure the shear strain directly to ensure the minimum influence of other deformation modes on experiment results. An INSTRON AVE (advanced non-contacting video extensometer) was used to measure the axial and transverse strain at the central region of the specimen during the test by tracking four white dots painted on the specimen surface in a cruciform pattern as shown in Fig. 10. Based on the trigonometric relationship, the measured shear angle γ_{exp} can be expressed as:

$$\gamma_{exp} = \frac{\pi}{2} - 2 \bullet \tan^{-1}\left(\frac{b}{a}\right) = \frac{\pi}{2} - 2 \bullet \tan^{-1}\left(\frac{b_0 \bullet (1+\varepsilon_b)}{a_0 \bullet (1+\varepsilon_a)}\right) \quad (4)$$

where a and b are axial and transverse separation between painted dots during the test (Fig. 10), a_0 and b_0 are initial axial and transverse separation between painted dots (gauge length) and ε_a and ε_b are axial and transverse strains acquired from the extensometer system. This measurement approach was applied to those tests where DIC was not used. Fig. 11 shows examples of the comparison between video extensometer obtained shear strain and theoretical shear strain determined using Eq. (2) for several tests. It is seen that the actual shear strain does not differ significantly from the theory at lower shear angles and the deviation becomes greater as shear angle increases. The load-extension data from the point where the measured shear strain deviates from the theoretical curve will be excluded from analysis in Section 3, due to the non-uniformity in shear strain distribution caused by additional deformation modes. Particularly, only the load-extension data below 5 mm and 3 mm crosshead displacement for 50 °C 0.00267/s and 50 °C 0.0107/s tests shown in Fig. 11 were selected for further processing and analysis.

The valid data ranges determined through shear angle comparison here and out-of-plane deformation in previous section only refer to the specific test rather than all tests in that test configuration. The data cut-off points were averaged for each test configuration and summarised in Fig. 12. In addition, any testing data with suspicious high force were

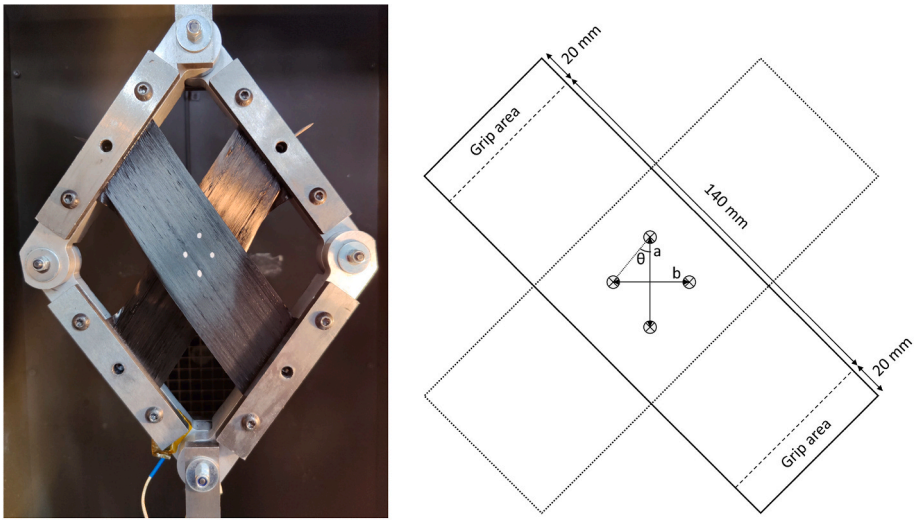

Fig. 10. Experimental shear angle measurement by tracking four dots on the specimen using a non-contacting video extensometer.

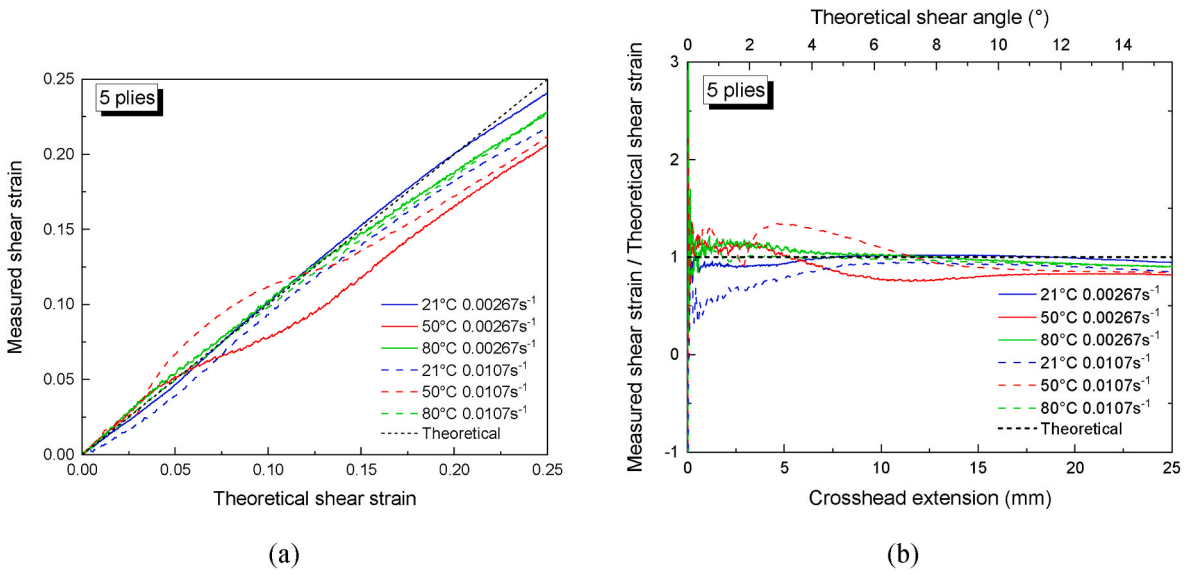

Fig. 11. Examples of theoretical and measured shear strain for 5-ply specimens: (a) a direct comparison, and (b) ratio of theoretical and measured shear strains vs. crosshead displacement and theoretical shear angles.

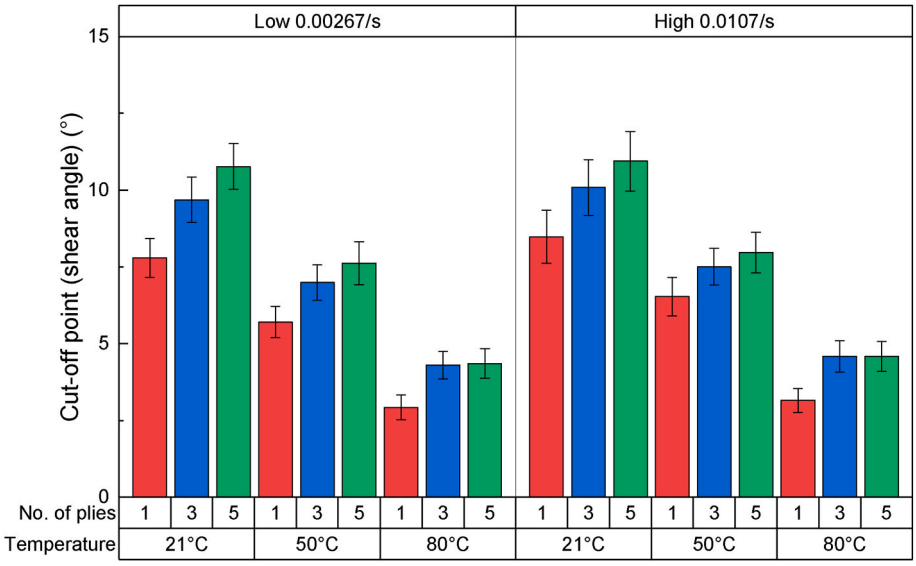

Fig. 12. Cut-off shear angles for all test configurations for 50 mm wide specimens.

excluded from further analysis to prevent the influences of fibre tension or misalignment.

2.7. Shear stress calculation

The shear force F_s can be calculated from the load data of the picture-frame test and normalised in terms of specimen and rig sizes as follows:

$$F_s = \frac{F}{2 \bullet \cos\theta} \tag{5}$$

$$F_{norm} = F_s \cdot \frac{L_{frame}}{L_{eff}^2} \tag{6}$$

where F is the net load (subtracting the 'dry run' empty fixture loads from the load data of actual tests) testing machine and L_{eff} is the effective length of specimen and, according to the assumed uniform shear distribution for the selected data range, can be expressed as [35]:

$$L_{eff} = \sqrt{2 \bullet w_0 \bullet L_{frame}} \tag{7}$$

Finally based on the above assumption of uniform shear strain field, the shear stress τ can be expressed as:

$$\tau = \frac{F_{norm}}{t} \tag{8}$$

where t is the thickness of specimen. The shear rigidity of the material as a function of the shear angle/strain can then be obtained by taking the first derivative of shear stress-strain curves [10]. The computed shear rigidity function can be used in the numerical simulation of the forming process for fabrics or prepregs [10,11,36].

3. Experimental results

3.1. Effects of specimen sizes

The shear kinematics and wrinkling response of engineering fabrics are size-dependent as shown in Ref. [37]. Therefore, it is important to investigate the potential size-effects on the intra-ply shear behaviour of UD prepreg such that the appropriate specimen configuration can be recommended and shear properties from the test can be applied in the simulation with confidence. By using the picture-frame test to characterise the intra-ply shear behaviour, this can be easily investigated by adjusting the width and thickness of UD prepreg specimens. Fig. 13 shows normalised shear forces for 1-ply specimens tested at 21 °C and 0.00267/s. The solid lines represent averaged results for all test repeats with the same specimen configuration and the coloured bands indicate calculated standard deviation. The normalised shear force has shown a similar trend and some overlaps for three different specimen widths. However, narrower specimens show higher normalised shear force, especially at very low strain where there is no overlay for the curves corresponding to different widths. Although narrower specimens are geometrically more resistant to transverse buckling, they can be more sensitive to disturbances from undesired forces, especially the tension in fibres caused by misalignment. This is indicated by the larger error bands for narrower 15 mm wide specimens and the rapid increase of normalised shear force from 8° shear angle for 25 mm and 15 mm wide specimens. Further, it was noticed in the experiment that it is more difficult to align the short edge of a narrower specimen with the rig when installing the specimens. This might have in turn contributed to higher normalised force for 15 mm wide specimens. Therefore, specimens with a width of 50 mm were selected for the test campaign for shear property characterisation.

The major advantage of using the purpose designed picture-frame rig to characterise the intra-ply shear behaviour of UD prepregs is the elimination of possible inter-ply shear/friction. However, for thicker specimens with more than one ply, it is crucial to study the influence of the presence of a ply-ply interface on intra-ply shear response. Fig. 14 shows shear stress-strain curves with error bands (standard deviations) for three different ply configurations (1 ply, 3 plies and 5 plies) at two test conditions. As per the study of the effect of specimen width, curves for different thicknesses show a close trend in the same test conditions. Curves for 1-ply specimen deviate from other curves at small strain level at 21 °C and have larger error band at 50 °C. The former was caused by the premature buckling as thin prepreg sheets are extremely compliant in the transverse direction; the reason for the latter could be its high sensitivity to the disturbance from spurious forces. However, the variation of the shear stress-strain response in terms of the thickness of specimen is small compared to the scatter in material response for the same thickness. Therefore, no apparent influences of specimen thickness on the shear stress-strain response need to be considered. All curves and error range for three thicknesses were averaged and combined in the study of loading rate and temperature effects in next sections.

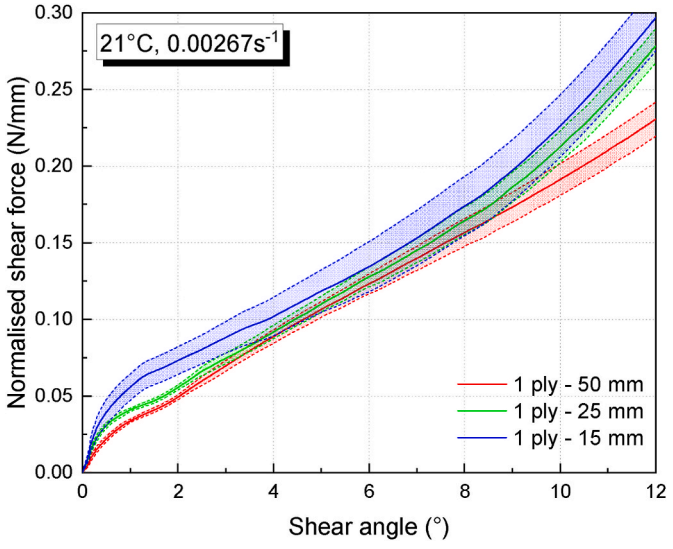

Fig. 13. Size effects study – normalised shear force vs. shear angle curves for specimens with three different widths (tested at 21 °C and 0.00267/s).

3.2. Effect of the loading rate

Fig. 15 shows shear stress-strain curves under two shear rates (0.00267/s and 0.0107/s) at each temperature (21 °C, 50 °C and 80 °C). It is worth noting that averaged curves are presented only up to the cut-off points for 1-ply specimens, which are the lowest values, as indicated in Fig. 12. In each case, the solid line represents the average shear stress-strain curve and the coloured band represents the lower and upper values of shear stress from all valid test repeats under the same test rate. The shear stress-strain response shows a non-linear relationship and the gradient of curves decreases with increased shear strain. For all temperatures, specimens experience higher shear stresses at high shear rate and the curves obtained from high loading rate tests show a larger linear portion at the start. These can be related to the viscoelastic behaviour of the uncured prepreg: a delayed viscous response will occur after a prominent linear response in the beginning of the test. At the microscales, the intra-ply shear deformation of UD prepregs can be regarded as the relative sliding between individual fibres with the lubrication of resin. In this intra-ply shear study, although the shear thinning of resin may decrease the viscosity of resin at the higher strain rate [38], the viscous resin is still able to transfer higher load between stiff fibres, resulting in higher shear stresses. This suggests a hydrodynamic (full-film) lubrication mode for the interaction between fibres in an uncured prepreg, which is in accordance with the findings from the study on friction behaviour of UD prepreg at macroscale [39]. At macroscale there is no indication of the rate effect on deformation modes from the comparison of specimens tested at low and high strain rate (Fig. 16 (a) and (b)).

3.3. Effect of temperature

The same curves from above were replotted in Fig. 17 for easy interpretation of the temperature effects. The shear stress-strain curves for different temperatures are plotted for each of the two strain rates. The results show a more profound influence of temperature on the shear response compared to the strain rate. There is a much greater difference in shear stress results between 21 °C and 50 °C than between 50 °C and 80 °C, which is in line with the viscosity profile of the epoxy resin considered in this study (Fig. 1 (b)). In addition, as shown in Fig. 16 (a), specimens tested at higher temperatures (50 °C and 80 °C) exhibit less wrinkling than specimens tested at room temperature in terms of both out-of-plane deformation and the number of wrinkles. This is caused by the local fibre/ply-splitting, shown as displaced gridlines highlighted in Fig. 16 (b), spread across the whole area of the specimen as the less viscous resin is less able to transfer the load between fibres at these temperatures. In the standard picture-frame test with cross-plied specimens, the local fibre/ply-splitting may be reduced to some extent, especially at room temperature, in the overlapping region (Fig. 5 (b)–(d)). This reduction in ply-splitting can also contribute to the higher forces observed for cross-plied specimens than proposed separated UD specimens.

Observations at microscale were performed to check the quality of consolidation and if there was any thick resin layer at ply-ply interface to provide lubrication or add resistance as well as possible fibre/ply-splitting. For these observations at microscale, untested specimens and specimens tested at 80 °C and 0.0107/s were cured in an oven in the free

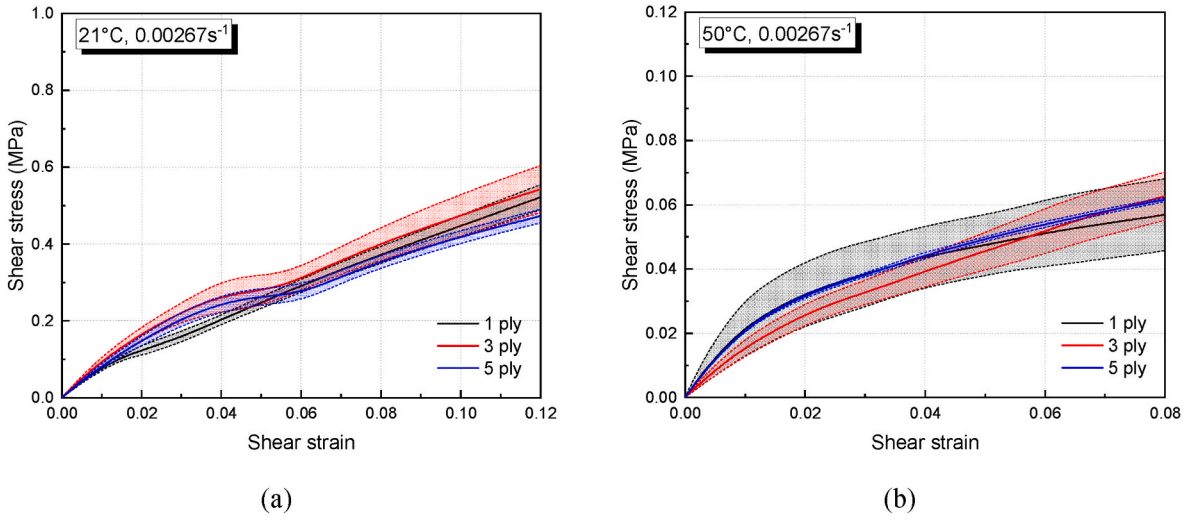

Fig. 14. Size effects study – shear stress vs. shear strain curves for specimens with different number of plies: tested at (a) 21 °C and 0.00267/s and (b) 50 °C and 0.00267/s.

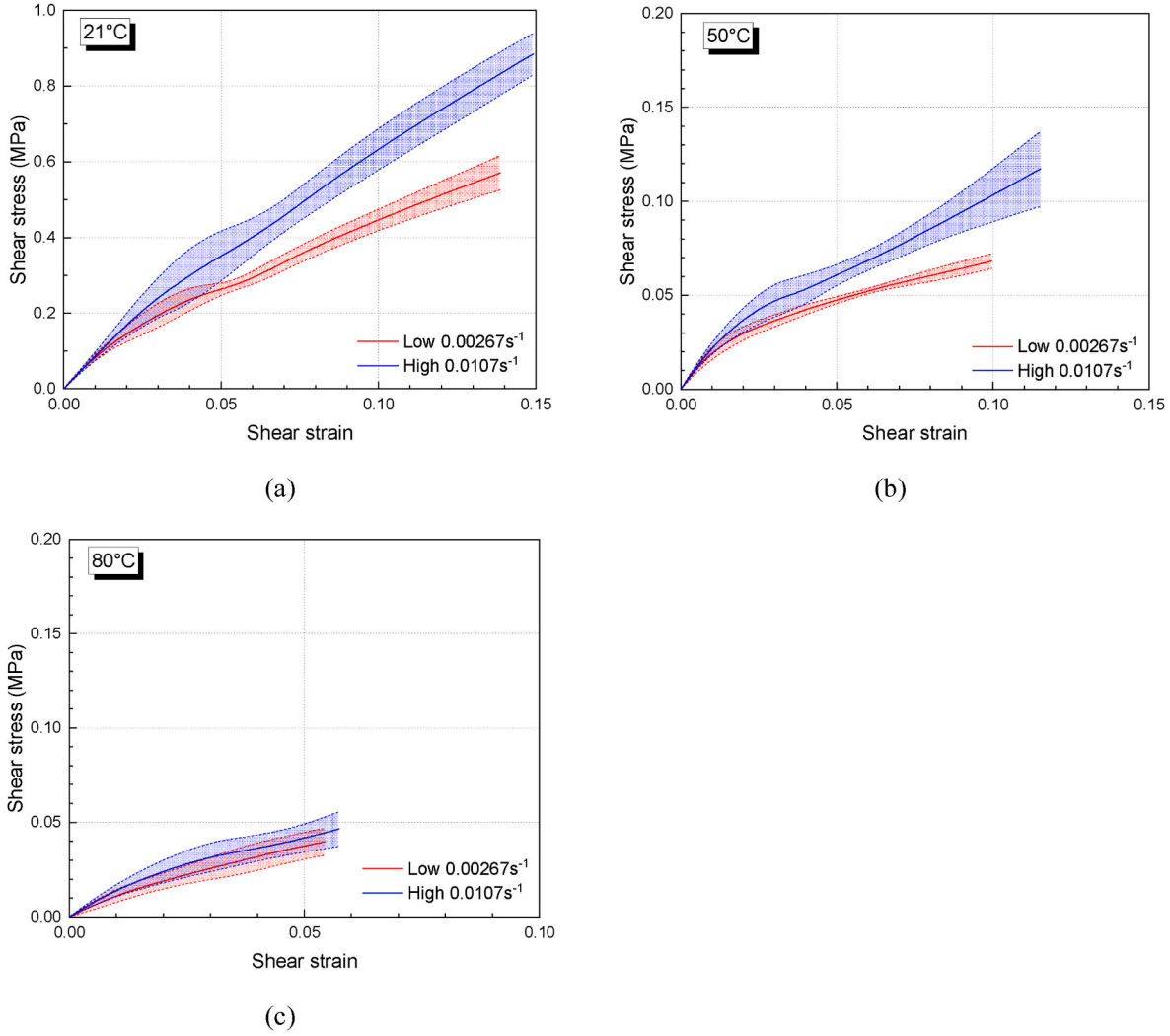

Fig. 15. Effect of the loading rate on the shear stress-strain response at (a) 21 °C, (b) 50 °C and (c) 80 °C.

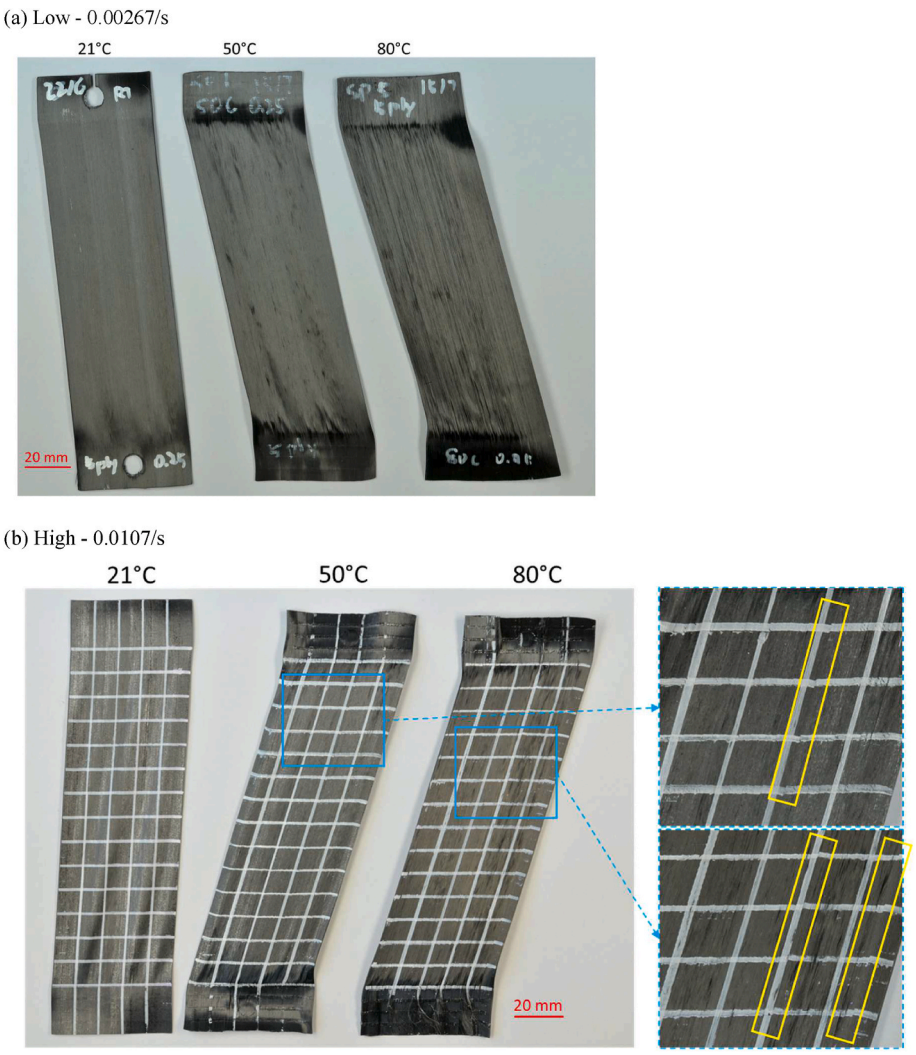

Fig. 16. 5-ply specimens after the test showing deformation modes (wrinkling and local fibre-splitting) for two different rates: (a) low – 0.00267/s and (b) high – 0.0107/s (with gridlines).

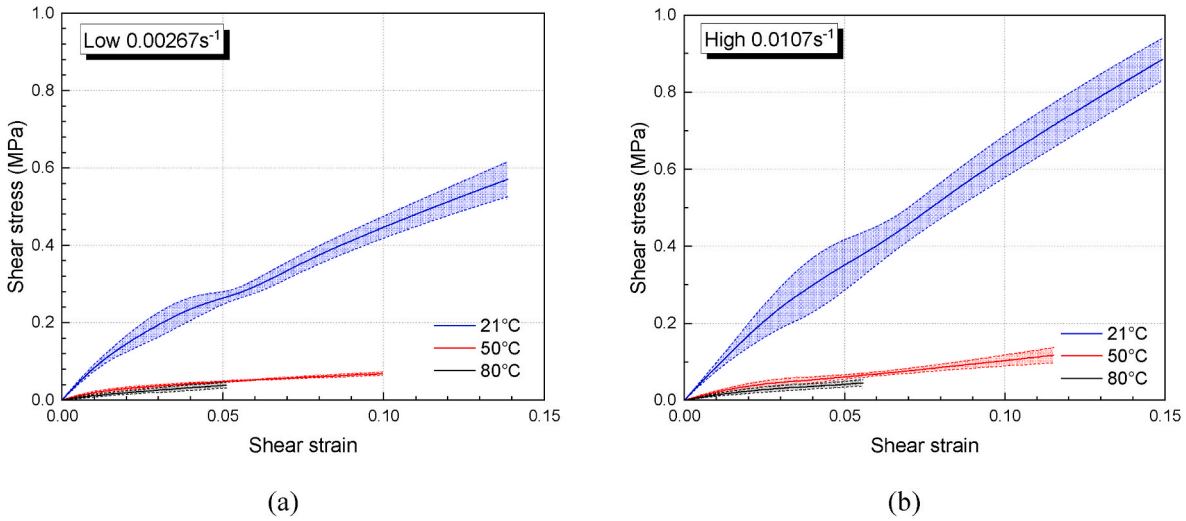

Fig. 17. Effect of temperature on shear stress-strain response at shear rates of (a) 0.00267 s^{-1} and (b) 0.0107 s^{-1}..

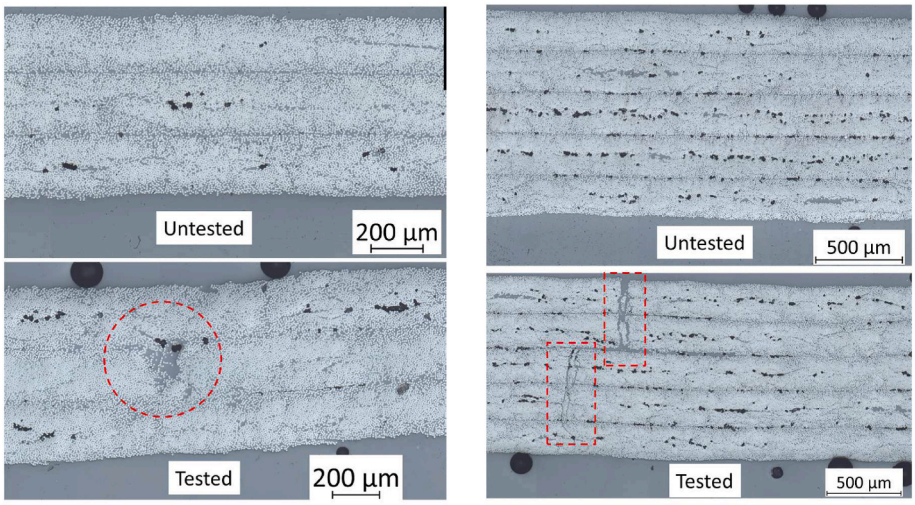

Fig. 18. Micrographs of cross-sections of untested specimens and specimens tested at 80 °C and 0.0107s^{-1} shear rate: (a) 3-ply specimen and (b) 5-ply specimen (dashed lines highlight fibre/ply-splitting).

air and cut by a CompCut 200 composite specimen cutter. The cross-section surface then was polished on a Buehler AutoMet™ 300 Pro grinder-polisher. Fig. 18 shows micrographs of the cross-section for untested and tested specimens of two thicknesses (3 plies and 5 plies) acquired using a Zeiss Axio Imager microscope. The fibre-splitting can also be observed from the highlighted area in the micrograph. The splitting in the middle ply (Fig. 18 (a)) suggests that splitting can still occur in non-surface plies and Fig. 18 (b) shows a more severe splitting across multiple plies. It is proposed that such local fibre-splitting is one reason for the early occurrence of shear non-uniformity, as the material obviously loses in-plane integrity in the transverse direction once the splitting occurs.

4. Numerical investigation of the picture-frame test

4.1. Hypoelastic approach for UD prepreg

The hypoelastic approach expressed as a rate constitutive law is one of the commonly adopted approaches for modelling the mechanical response of fibrous materials (e.g. fabrics and prepregs) with a 2D continuum constitutive model through ABAQUS user material subroutine VUMAT [11]. Due to the use of the objective rate, hypoelastic approach enables multiple possible frames and objective derivatives to be considered and stress can remain unchanged in case of the rigid body motion [40,41]. The strain rate $\underline{\underline{D}}$, is related with an objective stress derivative, using a tangent stiffness matrix, $\underline{\underline{\underline{\underline{C}}}}$:

$$\underline{\underline{\sigma}}^{\nabla} = \underline{\underline{\underline{\underline{C}}}} : \underline{\underline{D}} \tag{9}$$

where $\underline{\underline{\sigma}}^{\nabla}$ is an objective derivative of Cauchy stress $\underline{\underline{\sigma}}$. In such a hypoelastic law, the objective derivative is commonly based on the Green-Naghdi (GN) polar rotation tensor, however, the objective derivative for fibrous materials must be based on the fibre direction. It is defined with respect to the fibre rotation as [42]:

$$\underline{\underline{\sigma}}^{\nabla} = \underline{\underline{\Delta}} \bullet \left(\frac{d}{dt} \left(\underline{\underline{\Delta}}^{T} \bullet \underline{\underline{\sigma}} \bullet \underline{\underline{\Delta}} \right) \right) \bullet \underline{\underline{\Delta}}^{T} \tag{10}$$

where $\underline{\underline{\Delta}}$ is the rotation from the initial frame to fibre frame. Therefore, a further rotation is required for the hypoelastic law to be applied in the fibre frame caused by rigid body rotation of fibre yarns in large shearing. As shown in Fig. 19, the hypoelastic approach is based on a local

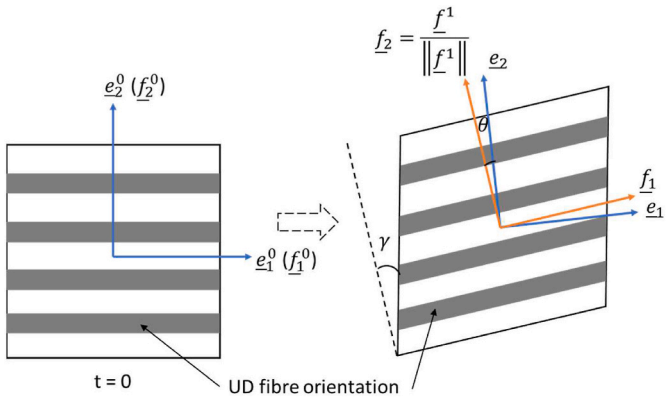

Fig. 19. Hypoelastic law code work frame (Green-Naghdi frame) ($e(\underline{e}_1, \underline{e}_2)$) and material/fibre frame ($f(\underline{f}_1, \underline{f}_2)$) for UD prepreg. Both frames are superimposed at t = 0: $\underline{f}_\alpha^0 = \underline{e}_\alpha^0$, where $\alpha = 1, 2$. (For interpretation of the references to colour in this figure legend, the reader is referred to the Web version of this article.)

orthogonal coordinate system (Green-Naghdi frame) $e(\underline{e}_1, \underline{e}_2)$. In case of unidirectional fibrous material, one fibre/material frame $f(\underline{f}_1, \underline{f}_2)$ is used, where $\underline{f}_1$ is the fibre axis and $\underline{f}_2 = \underline{f}^1 / \|\underline{f}^1\|$ is the in-plane unit vector orthogonal to the fibre direction, where $\underline{f}^1 \bullet \underline{f}_1 = \mathbf{0}$. The fibre axis can be expressed as:

$$\underline{f}_1 = \frac{\underline{\underline{F}} \bullet \underline{f}_1^0}{\left\| \underline{\underline{F}} \bullet \underline{f}_1^0 \right\|} = \frac{\underline{\underline{F}} \bullet \underline{e}_1^0}{\left\| \underline{\underline{F}} \bullet \underline{e}_1^0 \right\|} \tag{11}$$

where $\underline{f}_\alpha^0$ is aligned with the GN axes $\underline{e}_\alpha^0$ ($\alpha = 1, 2$) at the start. The strain increment, $[d\varepsilon]_e$, received in the GN frame at each increment is then transferred to the fibre frame:

$$[d\varepsilon]_f = [T]^T [d\varepsilon]_e [T] \tag{12}$$

where $[T]$ is the transformation matrix formed between GN frame and fibre frame. Following the strain increments transformed to the fibre directions, the stress increments along the fibre direction are calculated using a constitutive tensor, $[C]_f$:

$$[d\boldsymbol{\sigma}]_f = [\boldsymbol{C}]_f [d\boldsymbol{\varepsilon}]_f \tag{13}$$

Finally the stresses in the fibre frame are transformed back to GN frame for the codework in ABAQUS/Explicit:

$$[\boldsymbol{\sigma}]_e = [\boldsymbol{T}][\boldsymbol{\sigma}]_f [\boldsymbol{T}]^T \tag{14}$$

4.2. FE model

An FE model of the picture frame test was set up in ABAQUS/Explicit to validate the use of the hypoelastic approach in modelling the intra-ply shear response of UD prepreg (Fig. 20). The specimen dimensions were considered the same as in the experiment and a global element size of 2 mm was used for the specimen after the mesh convergence study. To set the same boundary conditions as in the experiment, nodes along both short edges of the specimen were fixed in z-direction and velocities in x- and y-direction as a function of time were applied to each node on these two edges. The required crosshead speed $\dot{d}$ to achieve a specific shear rate $\dot{\gamma}$ can be calculated using Eq. (3) and the velocities in x- and y-direction for each node have been carefully calculated based on the application of simple kinematic equations.

The bending stiffness of fibrous materials is not directly related to its in-plane properties and significantly lower than the in-plane tensile stiffness especially in the fibre direction, hence it cannot be directly characterised by the conventional three-point bending test. In this study, the bending stiffness used in the simulation was characterised for the same UD prepreg in a previous study [2] using simple cantilever beam method following [43]. It is important to consider the bending stiffness in the modelling of the picture-frame test for UD prepreg as it contributes to specimen's transverse buckling and the non-uniformity of shear distribution. To decouple the weak out-of-plane stiffness from high in-plane properties in the model, the superimposed membrane (M3D4R) and shell elements (S4R) sharing same nodes were used (Fig. 21). This method showed successes in predicting the bending behaviour of fibrous materials in the forming simulation [14,44]. Only the out-of-plane bending stiffness is applied to shell elements while all in-plane properties are stored in membrane elements. The flexural modulus E_f assigned to shell elements is determined based on Euler-Bernoulli theory:

$$E_f = \frac{12D}{t^3} \tag{15}$$

where D is the bending rigidity per unit width determined from the cantilever bending test and t is the thickness of the material. The

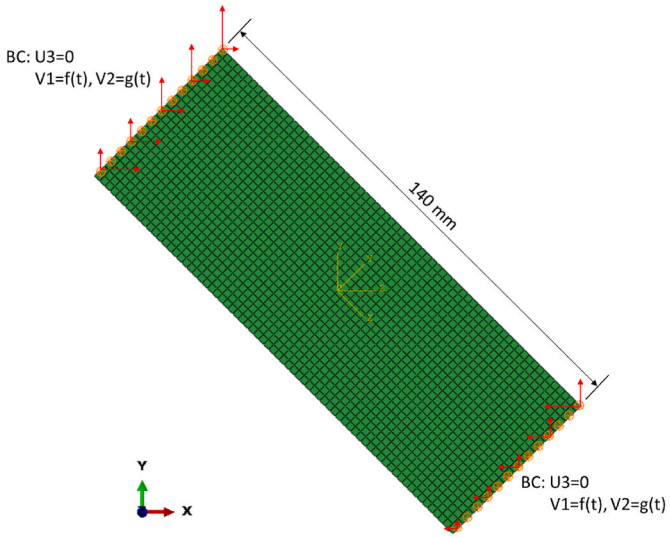

Fig. 20. FE model of the picture frame test.

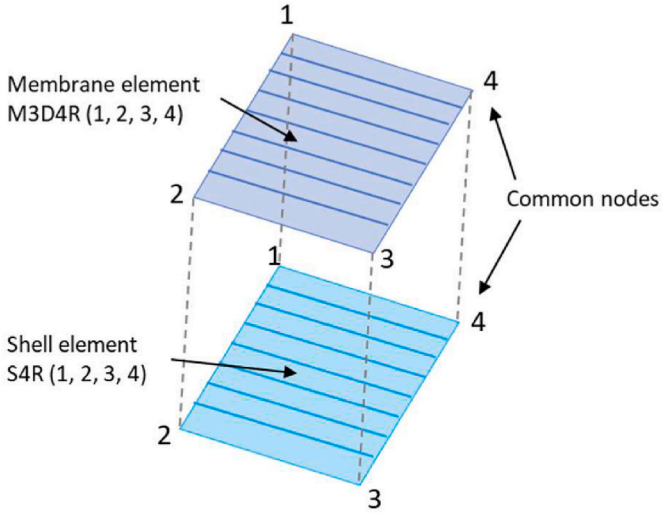

Fig. 21. Superimposed membrane and shell elements sharing the same nodes.

hypoelastic approach described in section 4.1 was implemented on both types of elements through VUMAT to account for the directionality of all mechanical properties of the UD prepreg.

The experimental results presented in the form of shear stress versus shear strain shown in Figs. 15 and 17 were used to derive the in-plane shear properties for the material in the FE model. By fitting the stress-strain results with a 5th order polynomial curve a polynomial regression equation can be obtained with shear stress as a function of shear strain. Taking derivative of this function gives another polynomial equation in the form of shear rigidity G_{12} as function of shear angle γ:

$$G_{12} = a_0 + a_1 \bullet \gamma + a_2 \bullet \gamma^2 + a_3 \bullet \gamma^3 + a_4 \bullet \gamma^4 + a_5 \bullet \gamma^5 \tag{16}$$

This was conducted for each test condition and the coefficients for the equation are presented in Table 2. Except the shear rigidity, other material properties required for the simulation (as summarised in Table 3) are from the characterisation studies for the same material and the material data were validated through simulation of corresponding tests and comparison of the outputs [2]. The tensile stiffness of the material has minimum influence on the results of the simulation of the trellis shear and a reasonably low value of 20 GPa can reduce the computational cost. Although bending stiffness can affect the shape of wrinkles, its effects on the resultant force in the exploratory simulation study were found to be negligible compared to the effects of in-plane shear properties. Similar to the simulation strategy adopted in Ref. [31], all other material properties are independent of the effects of temperature and loading rate, therefore, the differences between different numerical tests are the direct result of the variation of the shear property.

4.3. Simulation results and discussion

Fig. 22 shows a comparison of the shear angle and out-of-plane deformation results between DIC measurement and FE model at the same level of specimen extension for a test at 21 °C and under 0.00267/s shear rate. Compared to DIC results, the FE results show a relatively more uniform shear distribution at a later stage of the test Fig. 22 (a). The major reason is that this macroscale FE model has no means to capture the local fibre splitting phenomenon as presented in Fig. 16, as simulation results for all temperatures show only the macroscale defect of transverse buckling throughout the test. The out-of-plane deformation from FE model shows a similar pattern to DIC results in terms of the topology and number of wrinkles (Fig. 22 (b)), but the out-of-plane displacement is much smaller from the simulation (note that the colour scales are adjusted to enable comparison). This can be attributed

Table 2
Coefficients of polynomial equations for in-plane shear rigidity G_{12} (Eq. (16)) for different temperatures and shear rates.

		a_0	a_1	a_2	a_3	a_4	a_5
Low 0.00267 s^{-1}	21 °C	10.4017	−411.604	9057.16	−91007.6	419973	−724130
	50 °C	10.5573	−272.559	5585.40	−52755.6	227286	−361158
	80 °C	2.22466	−98.6047	2068.00	−20606.3	96720.2	−171997
High 0.0107 s^{-1}	21 °C	3.28915	−146.987	3224.99	−32522.5	152138	−268212
	50 °C	1.35365	−34.3822	562.706	−5161.38	24092.7	−43619.2
	80 °C	2.25654	−80.2348	1395.03	−11589.2	45654.6	−69588.9

Table 3
Material properties for the respective elements in FE model.

	E_1 (MPa)	E_2 (MPa)	G_{12}
Membrane (M3D4R)	20,000	0.25	Eq. (16)
Shell (S4R)	3500	0.2	0

to those factors that influence the bending stiffness but are not considered in the FE model: the effects of element sizes, prepreg's viscoelastic bending behaviour and the nonlinearity of bending stiffness for fibrous materials in terms of the curvature.

To validate the numerical picture-frame test, the load-extension curves at different temperatures and loading rates for 3-ply and 5-ply specimens were extracted and compared with the physical test data. The reaction force in vertical/y-direction for all 26 nodes along the top edge was extracted and summed up. This total reaction force for one specimen was doubled to allow comparisons with experimental data from the perpendicularly mounted dual specimen geometry (Fig. 23). The load-extension curves from the FE model show a good level of agreement with the experiment results at the beginning of the test (small shear strains). In contrast, the simulation results for the 5-ply specimen at higher temperatures show lower forces than the experimental results in this beginning stage (Fig. 23 (e) and (f)), which can be attributed to less predominant effects of fibre splitting and higher buckling resistance for 5-ply specimens compared to thinner specimens. The experimental stress-strain curves for 1-ply and 3-ply specimens could be more sensitive to the effects of fibre splitting compared to 5 plies due to less constraints from additional plies and this can start from the very beginning of the test once specimens were loaded. In addition, the cut-off points or the buckling onsets can differ by more than 3° (0.052 shear strain) for the same test condition but different number of plies as shown in Fig. 12. However, the shear property curves used in the simulation are the average result for three thicknesses and contain above effects from specimens with fewer plies, hence, the simulation result curves for 5-ply specimens can be more compliant than experimental results in the beginning of the test.

In a later stage of the test, the load required to deform the specimen starts to deviate from the experiment curves from 5 mm crosshead displacement. The lack of local fibre splitting in the FE model plays a role in this. In addition, as the velocity boundary conditions were applied as 1000 discrete points over the required step time rather than a continuous curve, the rigid body motion in the picture-frame numerical test may not be perfectly achieved, leading to small levels of tension in elements at higher strains. Further, by modelling only one specimen in the numerical tests, it was assumed that the unmodelled second specimen would behave exactly the same. In the physical experiments, two specimens in one test usually show slightly different patterns due to the handling issue and material variation between specimens.

5. Conclusions

The feasibility of using a modified picture-frame test for intra-ply shear characterisation of UD prepreg was investigated in this study, implementing only modest changes to the standard apparatus with the aim of completely eliminating the confounding influence of inter-ply shear/friction as experienced in the standard picture-frame test with cross-plied specimens. 3D DIC techniques and non-contacting video extensometers were used with the modified picture frame testing to determine the uniformity of shear distribution and onset of non-preferred deformation modes throughout testing and therefore identify valid ranges of test data. Specimens showed relatively uniform shear deformation at lower strains, after which the transverse buckling/wrinkling and local splitting disrupted the shear deformation – these non-preferred deformation modes arise from greatly reduced in-plane shear compliance because of transverse compaction. From the study of specimen size effects, narrower and thinner specimens showed greater variation in the normalised results, suggesting a higher instability of the specimen due to their low resistance to transverse buckling and possible initial misalignment of specimens/fibres. Therefore, wider specimens with multiple plies are recommended for any future intra-ply shear tests using this proposed approach. The shear stress-strain curves exhibited a typical viscoelastic response as the material experiences higher stress at lower temperatures and higher shear rate. Temperature shows a stronger influence on stress-strain response than the shear rate due to the large drop of resin viscosity at higher temperatures. This also resulted in local fibre splitting at microscale which is the dominant additional deformation mode rather than transverse wrinkling.

A numerical model of the picture-frame test was built and analysed using ABAQUS/Explicit to validate the proposed method for obtaining in-plane shear properties for simulation. The experimental stress-strain data was fitted by polynomial regression equations to derive the in-plane shear rigidity as a function of shear strain for different test conditions. This property was applied to the superimposed membrane-shell elements by the hypoelastic constitutive law implemented through a VUMAT subroutine. The proposed approach predicted the reaction force with a high degree of correlation (to physical test data) at low strain levels but the predicted load is higher at large shear strains due to the inability of the model to capture local fibre splitting and possibly imperfect rigid body rotation achieved by velocity boundary conditions. Overall, the load-extension curves from the simulations showed a good level of agreement with the experimental data, verifying the data obtained through the proposed approach for characterisation of intra-ply shear behaviour of UD prepreg and building confidence towards adopting a modelling approach for the future forming simulation work of UD prepreg at component level.

This work lays a foundation for a comprehensive characterisation study of intra-ply shear behaviour for UD prepregs under real-world forming conditions. Further work will include exploring of the possibility of capturing the local fibre-splitting phenomena (or its effect) into the simulation model so that more accurate force prediction can be achieved at higher shear strains. Finally, additional tests should be done across a range of temperatures and strain rates within the range of industrial processing conditions to fully parameterise the effect of the viscoelastic resin behaviour thus leading to the development of a robust model for intra-ply shear behaviour.

CRediT authorship contribution statement

H. Yuan: Investigation; Methodology; Data curation; Formal analysis; Software; Validation; Visualisation; Writing – original draft. M. A.

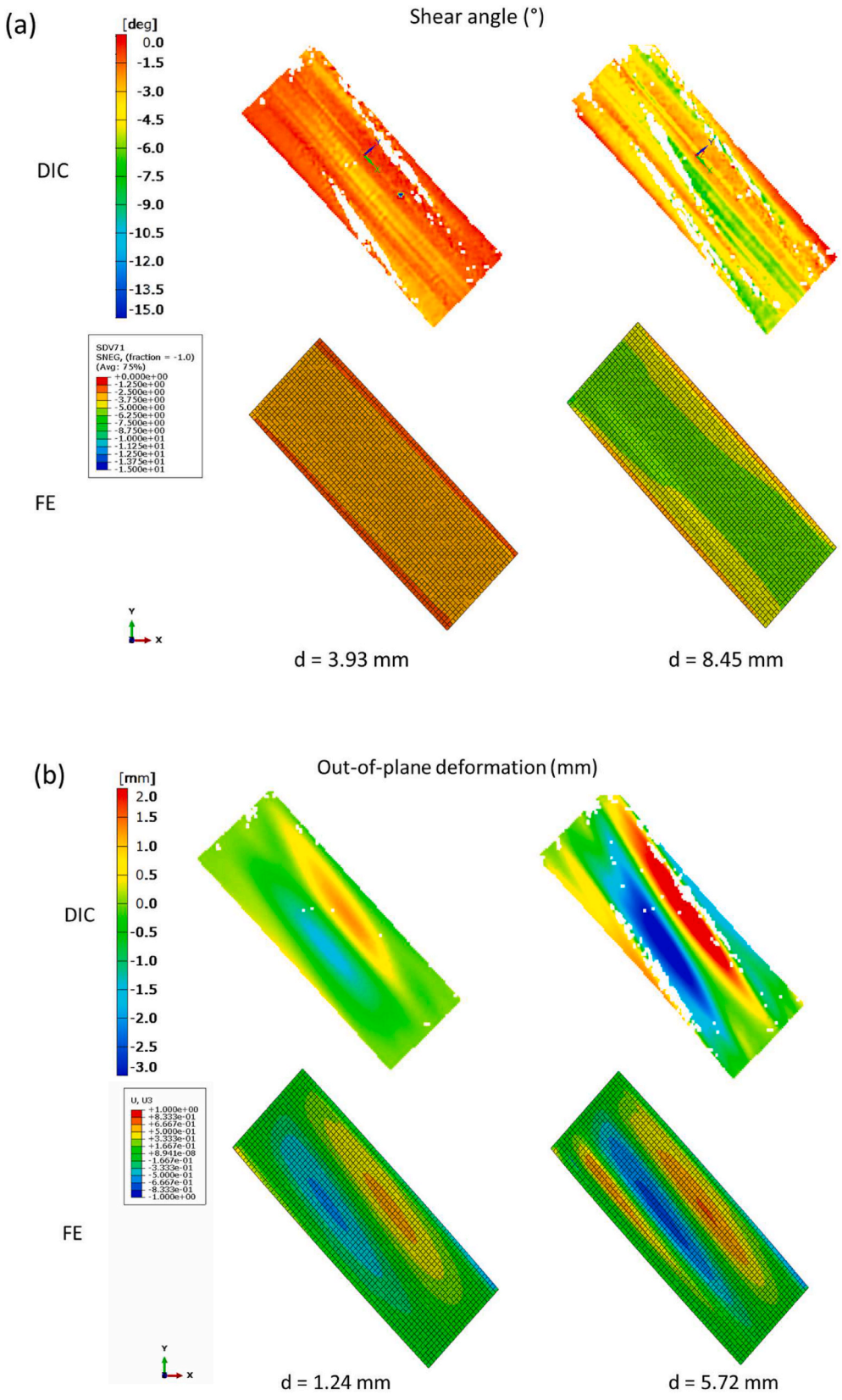

Fig. 22. Comparison of (a) shear angle (SDV71 is the shear angle in degrees) and (b) out-of-deformation results between DIC and FE model for the test at 21 °C and 0.00267 s^{-1} shear rate (colour scales are adjusted to enable comparison). (For interpretation of the references to colour in this figure legend, the reader is referred to the Web version of this article.)

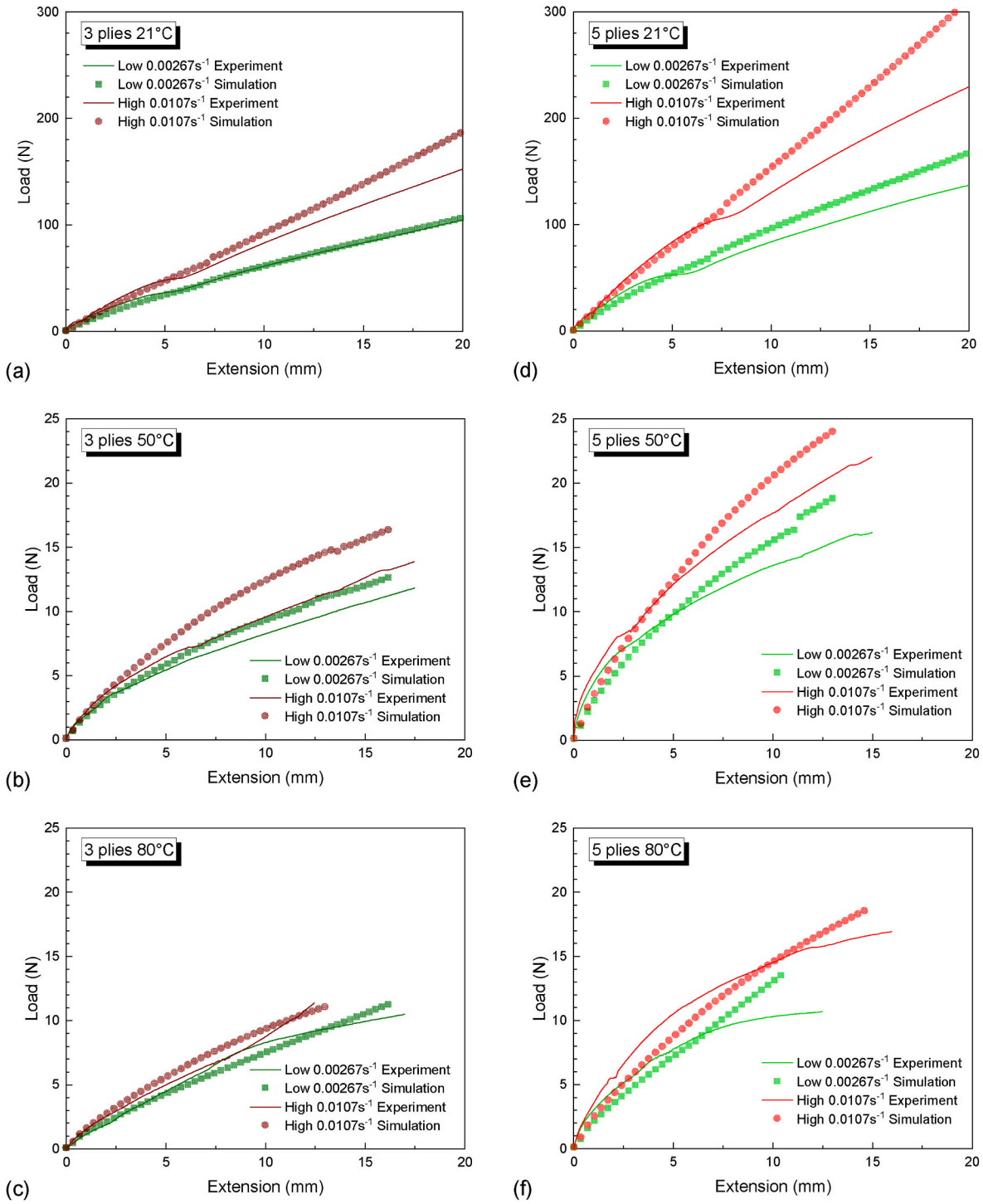

Fig. 23. Comparison of load-extension results between experiment and simulation for 3-ply and 5-ply specimens at different temperatures and shear rates.

Khan: Conceptualisation; Methodology; Supervision; Validation; Writing – review & editing. C. C. Qian: Resources, Supervision, Project administration. N. C. Reynolds: Investigation; Validation; Writing – review & editing. K. N. Kendall: Project administration; Resources, Supervision.

Declaration of competing interest

The authors declare that they have no known competing financial interests or personal relationships that could have appeared to influence the work reported in this paper.

Data availability

Data will be made available on request.

Acknowledgement

The authors acknowledge the support from EPSRC United Kingdom through Researcher-in-Residence program and HVM CATAPULT (Ref. EP/R513581/2). The authors would also like to thank the support from China Scholarship Council (CSC).

References

[1] Henning F, Kärger L, Dörr D, Schirmaier FJ, Seuffert J, Bernath A. Fast processing and continuous simulation of automotive structural composite components. Compos Sci Technol 2019;171:261–79. https://doi.org/10.1016/j.compscitech.2018.12.007.

[2] Pasco CE. Prepreg forming numerical analysis and experimental characterisation for a novel high- volume forming process. PhD Thesis. University of Warwick; 2018. http://wrap.warwick.ac.uk/151031/.

[3] Boisse P, Akkerman R, Carlone P, Kärger L, Lomov SV, Sherwood JA. Advances in composite forming through 25 years of ESAFORM. Int J Material Form 2022;15. https://doi.org/10.1007/s12289-022-01682-8.

[4] Yu F, Chen S, Lawrence GD, Warrior NA, Harper LT. A global-to-local sub modelling approach to investigate the effect of lubrication during double diaphragm forming of multi-ply biaxial non-crimp fabric preforms. Compos Part B Eng 2023;254:13–6. https://doi.org/10.1016/j.compositesb.2023.110590.

[5] Harrison P, Clifford MJ, Long AC. Shear characterisation of viscous woven textile composites: a comparison between picture frame and bias extension experiments. Compos Sci Technol 2004;64:1453–65. https://doi.org/10.1016/j.compscitech.2003.10.015.

[6] Cao J, Akkerman R, Boisse P, Chen J, Cheng HS, de Graaf EF, et al. Characterization of mechanical behavior of woven fabrics: experimental methods and benchmark results. Compos Part A Appl Sci Manuf 2008;39:1037–53. https://doi.org/10.1016/j.compositesa.2008.02.016.

[7] Boisse P, Hamila N, Guzman-Maldonado E, Madeo A, Hivet G, dell'Isola F. The bias-extension test for the analysis of in-plane shear properties of textile composite reinforcements and prepregs: a review. Int J Material Form 2017;10:473–92. https://doi.org/10.1007/s12289-016-1294-7.

[8] Khan MA, Pasco C, Reynolds N, Kendall K. Shear deformability characteristics of a rapid-cure woven prepreg fabric. Int J Material Form 2020. https://doi.org/10.1007/s12289-019-01532-0.

[9] Mattner T, Wrensch M, Drummer D. Shear behavior of woven and non-crimp fabric based thermoplastic composites at near-processing conditions. Compos Part B Eng 2020;185:107761. https://doi.org/10.1016/j.compositesb.2020.107761.

[10] Hamila N, Boisse P. Simulations of textile composite reinforcement draping using a new semi-discrete three node finite element. Compos Part B Eng 2008;39:999–1010. https://doi.org/10.1016/j.compositesb.2007.11.008.

[11] Khan MA, Mabrouki T, Vidal-Sallé E, Boisse P. Numerical and experimental analyses of woven composite reinforcement forming using a hypoelastic behaviour. Application to the double dome benchmark. J Mater Process Technol 2010;210:378–88. https://doi.org/10.1016/j.jmatprotec.2009.09.027.

[12] Boisse P, Aimène Y, Dogui A, Dridi S, Gatouillat S, Hamila N, et al. Hypoelastic, hyperelastic, discrete and semi-discrete approaches for textile composite reinforcement forming. Int J Material Form 2010;3:1229–40. https://doi.org/10.1007/s12289-009-0664-9.

[13] Peng X, Guo Z, Du T, Yu WR. A simple anisotropic hyperelastic constitutive model for textile fabrics with application to forming simulation. Compos Part B Eng 2013;52:275–81. https://doi.org/10.1016/j.compositesb.2013.04.014.

[14] Thompson AJ, Belnoue JPH, Hallett SR. Modelling defect formation in textiles during the double diaphragm forming process. Compos Part B Eng 2020;202:108357. https://doi.org/10.1016/j.compositesb.2020.108357.

[15] Wang Y, Chea MK, Belnoue JPH, Kratz J, Ivanov DS, Hallett SR. Experimental characterisation of the in-plane shear behaviour of UD thermoset prepregs under processing conditions. Compos Part A Appl Sci Manuf 2020;133:105865. https://doi.org/10.1016/j.compositesa.2020.105865.

[16] Groves DJ. A characterization of shear flow in continuous fibre thermoplastic laminates. Composites 1989;20:28–32. https://doi.org/10.1016/0010-4361(89)90678-2.

[17] Groves DJ, Bellamy AM, Stocks DM. Anisotropic rheology of continuous fibre thermoplastic composites. Composites 1992;23:75–80. https://doi.org/10.1016/0010-4361(92)90107-6.

[18] Scobbo JJ, Nakajima N. Modification of the mechanical energy resolver for high temperature and rigid material applications. Polym Test 1990;9:245–55. https://doi.org/10.1016/0142-9418(90)90011-2.

[19] Goshawk JA, Jones RS. Structure reorganization during the rheological characterization of continuous fibre-reinforced composites in plane shear. Compos Part A Appl Sci Manuf 1996;27:279–86. https://doi.org/10.1016/1359-835X(95)00049-8.

[20] Wheeler AB, Jones RS. A characterization of anisotropic shear flow in continuous fibre composite materials. Compos Manuf 1991;2:192–6. https://doi.org/10.1016/0956-7143(91)90139-8.

[21] Jones RS, Roberts RW. Anisotropic shear flow in continuous fibre composites. Composites 1994;25:171–6. https://doi.org/10.1016/0010-4361(94)90013-2.

[22] Roberts RW, Jones RS. Rheological characterization of continuous fibre composites in oscillatory shear flow. Compos Manuf 1995;6:161–7. https://doi.org/10.1016/0956-7143(95)95007-L.

[23] Dykes RJ, Martin TA, Bhattacharyya D. Determination of longitudinal and transverse shear behaviour of continuous fibre-reinforced composites from vee-bending. Compos Part A Appl Sci Manuf 1998;29:39–49. https://doi.org/10.1016/S1359-835X(97)00027-4.

[24] McGuinness GB, Ó Brádaigh CM. Characterisation of thermoplastic composite melts in rhombus-shear: the picture-frame experiment. Compos Part A Appl Sci Manuf 1998;29:115–32. https://doi.org/10.1016/S1359-835X(97)00061-4.

[25] Dangora LM, Hansen CJ, Mitchell CJ, Sherwood JA, Parker JC. Challenges associated with shear characterization of a cross-ply thermoplastic lamina using picture frame tests. Compos Part A Appl Sci Manuf 2015;78:181–90. https://doi.org/10.1016/j.compositesa.2015.08.015.

[26] Potter K. Bias extension measurements on cross-plied unidirectional prepreg. Compos Part A Appl Sci Manuf 2002;33:63–73. https://doi.org/10.1016/S1359-835X(01)00057-4.

[27] Larberg YR, Åkermo M, Norrby M. On the in-plane deformability of cross-plied unidirectional prepreg. J Compos Mater 2012;46:929–39. https://doi.org/10.1177/0021998311412988.

[28] Khan MA, Pasco C, Reynolds N, Kendall KN. On the validity of bias-extension test method for the characterisation of in-plane shear properties of rapid-cure prepregs. Compos Struct 2020;246:112399. https://doi.org/10.1016/j.compstruct.2020.112399.

[29] Haanappel SP, Akkerman R. Shear characterisation of uni-directional fibre reinforced thermoplastic melts by means of torsion. Compos Part A Appl Sci Manuf 2014;56:8–26. https://doi.org/10.1016/j.compositesa.2013.09.007.

[30] Potter K. In-plane and out-of-plane deformation properties of unidirectional preimpregnated reinforcement. Compos Part A Appl Sci Manuf 2002;33:1469–77. https://doi.org/10.1016/S1359-835X(02)00138-0.

[31] Wang Y, Belnoue JPH, Ivanov DS, Hallett SR. Hypo-viscoelastic modelling of in-plane shear in UD thermoset prepregs. Compos Part A Appl Sci Manuf 2021;146:106400. https://doi.org/10.1016/j.compositesa.2021.106400.

[32] Zhao Y, Zhang T, Li H, Zhang B. Characterization of prepreg-prepreg and prepreg-tool friction for unidirectional carbon fiber/epoxy prepreg during hot diaphragm forming process. Polym Test 2020;84:106440. https://doi.org/10.1016/j.polymertesting.2020.106440.

[33] Pasco C, Khan M, Kendall K. A novel discrete method of shear angle measurement for in-plane shear properties of thermoset prepreg using a point-tracking algorithm. J Compos Mater 2019;53:2001. https://doi.org/10.1177/0021998318813193. –13.

[34] National Institutes of Health. Image 1997.

[35] Peng XQ, Cao J, Chen J, Xue P, Lussier DS, Liu L. Experimental and numerical analysis on normalization of picture frame tests for composite materials. Compos Sci Technol 2004;64:11–21. https://doi.org/10.1016/S0266-3538(03)00202-1.

[36] Khan MA, Reynolds N, Williams G, Kendall KN. Processing of thermoset prepregs for high-volume applications and their numerical analysis using superimposed finite elements. Compos Struct 2015;131:917–26. https://doi.org/10.1016/j.compstruct.2015.06.056.

[37] Harrison P, Alvarez MF, Anderson D. Towards comprehensive characterisation and modelling of the forming and wrinkling mechanics of engineering fabrics. Int J Solid Struct 2018;154:2–18. https://doi.org/10.1016/j.ijsolstr.2016.11.008.

[38] Meier R, Kirdar C, Rudolph N, Zaremba S, Drechsler K. Investigation of the shear thinning behavior of epoxy resins for utilization in vibration assisted liquid composite molding processes. AIP Conf Proc 2014;1593:458–62. https://doi.org/10.1063/1.4873821.

[39] Pasco C, Khan M, Gupta J, Kendall K. Experimental investigation on interply friction properties of thermoset prepreg systems. J Compos Mater 2019;53:227–43. https://doi.org/10.1177/0021998318781706.

[40] Badel P, Vidal-Sallé E, Boisse P. Large deformation analysis of fibrous materials using rate constitutive equations. Comput Struct 2008;86:1164–75. https://doi.org/10.1016/j.compstruc.2008.01.009.

[41] Badel P, Gauthier S, Vidal-Sallé E, Boisse P. Rate constitutive equations for computational analyses of textile composite reinforcement mechanical behaviour during forming. Compos Part A Appl Sci Manuf 2009;40:997–1007. https://doi.org/10.1016/j.compositesa.2008.04.015.

[42] Boisse P, Gasser A, Hagege B, Billoet J-L. Analysis of the mechanical behavior of woven fibrous material using virtual tests at the unit cell level. J Mater Sci 2005;40:5955–62. https://doi.org/10.1007/s10853-005-5069-7.

[43] Peirce FT. The '"handle'" of cloth as a measurable quantity. J Text Inst Trans 1930;21:T377–416. https://doi.org/10.1080/19447023008661529.

[44] Dörr D, Schirmaier FJ, Henning F, Kärger L. A viscoelastic approach for modeling bending behavior in finite element forming simulation of continuously fiber reinforced composites. Compos Part A Appl Sci Manuf 2017;94:113–23. https://doi.org/10.1016/j.compositesa.2016.11.027.